

A Random Rule Model

Avner Seror*

Abstract

We propose a Random Rule Model (RRM) in which behavior is generated by switching among a small library of transparent, parameter-free decision rules. A differentiable gate learns environment-dependent rule propensities, producing an interpretable mixture over named procedures. We develop a global identification theory based on two verifiable conditions on the observed support. Applied to 10,000 binary lottery problems, rule-gating substantially outperforms structured neural benchmarks based on expected utility and prospect theory, approaching the most flexible benchmark while remaining highly restrictive under permutation-fit tests, and retains predictive content on an independent dataset. Mechanism diagnostics reveal that extreme-outcome screening, salience, and attention rules carry the largest responsibility weights, with systematic shifts along tradeoff complexity and dispersion asymmetry. Robustness checks confirm that the findings are not driven by the ex-ante library choice, marginal dominance relationships, or the availability of additional regressors.

Keywords: Behavioral Economics, Decision Theory, Random Rule Model, Identification, Risky Choice, Machine Learning.

JEL Classification: D81, C25, C52, D91.

1 Introduction

A central task in economics is to represent how behavior varies across environments. In many modern empirical settings, the environment space is vast: researchers observe thousands of distinct decision problems, often with repeated observations for each problem, and the main object of interest becomes the systematic mapping from a decision environment to behavior. One fundamental challenge is therefore not only to fit this mapping accurately - modern machine-learning predictors typically do - but to do so with a representation that remains economically interpretable and empirically disciplined.

This paper proposes a procedural representation of this mapping. Instead of assuming that choices are generated by a single valuation model, we model behavior as switching among a small library of transparent, deterministic decision rules. We call this representation a Random Rule

*Aix-Marseille University, CNRS, AMSE, Marseille, France. Email: avner.seror@univ-amu.fr. I am grateful to Marina Agranov, Benjamin Enke, En Hua Hu, Dotan Persitz, John Quah, and Thierry Verdier for helpful discussions. I acknowledge funding from the French government under the ANR JCJC "BIAS" project (reference: ANR-25-CE26-7164-01) and the "France 2030" investment plan managed by the French National Research Agency (reference: ANR-17-EURE-0020) and from the Excellence Initiative of Aix-Marseille University – A*MIDEX. Mistakes are my own. Parts of this manuscript were prepared with the assistance of large language models (Claude and GPT). Refine.ink was used to check the paper for consistency and clarity. The author used these tools for code development and editorial revisions; all scientific content, modeling choices, and results were produced and verified by the author.

Model (RRM): behavior in a given environment is as if one rule from the library is selected at random and its recommendation is followed. A differentiable gating mechanism assigns propensities to rules as a function of observable features of the environment, so that predicted behavior is an explicitly interpretable mixture over named lines of conduct. In this way, machine-learning optimization is used as a tool to estimate a disciplined economic structure - one that scales to large environments, does not presuppose rationality, and preserves a decomposition of fit into distinct behavioral mechanisms.

A Random Rule Model is attractive as a general representation of choice for at least three reasons. First, it provides an interpretable language for systematic heterogeneity across environments. When behavior changes with the decision problem, the model does not simply register a shift in a latent value function; it states which line of conduct becomes more prevalent and which becomes less so. This makes it possible to summarize large environment-to-behavior mappings in terms of a small set of well-studied behavioral mechanisms - e.g., screening on extremes, focusing on modal outcomes, salience-based comparisons, regret-type comparisons, limited consideration, and related procedures - without committing to a single parametric valuation story that must govern all environments.

Second, RRM impose a distinctive form of empirical discipline. The model can only fit the mapping from environments to behavior through the patterns of agreement and disagreement generated by the rule library, together with how these patterns vary with observable features. This restriction is neither the knife-edge discipline of a fully specified valuation model nor the unconstrained flexibility of a black-box predictor. It is instead a procedural discipline: the representation is flexible in where different procedures apply, but disciplined in what procedures can be invoked and in how they can combine. This makes RRM well suited to settings where the environment space is large and rich, but where interpretability requires that predictive success be attributable to a limited repertoire of transparent procedures.

A further advantage is that RRM do not presuppose the kind of cyclical consistency condition that underlies valuation-based representations. In large menu datasets, such restrictions are often violated, and it is empirically difficult to determine whether violations reflect measurement noise, instability of preferences, or heterogeneity in the latent valuation objects that could rationalize the data. By contrast, the RRM disciplines behavior procedurally. It allows rich non-transitive and context-dependent patterns in the induced choice relation, while keeping interpretation anchored in a transparent library of deterministic rules whose prevalence can vary systematically with observable features of the environment.

This procedural representation raises a foundational question: when is the gate - and hence the behavioral decomposition - pinned down by the data, rather than being a convenient reparameterization of a flexible predictor? We answer this by developing an identification theory for Random Rule Models. The key identifying force is *rule switching*: because a given rule recommends different sides in different decision problems, it links its latent index across many competitive configurations. We formalize this logic and show how identification reduces to a verifiable property of the realized design: global identification follows from two transparent conditions on the observed menu support: within-feature variation in decisive-side patterns (which rules recommend which side must vary enough at each feature value) and affine richness of the feature values at which this variation occurs. Both conditions are directly verifiable on the data. In our application, the gate operates on a 12-dimensional vector of interpretable summary statistics $z(A)$ - coarse enough that many distinct menus share the same feature value, making the within-feature conditions empirically

testable, while capturing the decision-relevant variation without sacrificing predictive accuracy.

Identification matters because the empirical object of interest is not only predictive accuracy, but an interpretable procedural decomposition: which named procedures are operative, and how their prevalence shifts with primitive features of the environment. The RRM structure makes this decomposition explicit. For each environment, the model first determines which rules are *active*—i.e., which procedures deliver a strict ranking under the model’s dominance - based decisiveness criterion — then the gate outputs weights across the active rules. Predicted behavior is therefore an explicit mixture of rule-generated recommendations with environment-dependent mixture weights. This structure turns fit into mechanism-level objects: (i) how many rules are typically decisive, (ii) how responsibility is distributed across economically meaningful families of procedures, and (iii) how responsibility shifts with salient features of the environment. Without identification, these decompositions would be fragile; with it, they become disciplined, data-supported statements about procedural variation.

Although the framework applies to general discrete choice environments with arbitrary menu sizes and dominance criteria, we develop this fully in Appendix A, where we state and prove the global identification theorem for menus with finitely many alternatives (Theorem 2). The main text presents the model, identification theory, and diagnostics in the binary choice setting. This is without loss of generality for the conceptual development: the general and binary treatments share the same structure - a grouped-softmax representation, activity-conditional normalization, and verifiable conditions for global identification - with the main difference being notational (log-odds become log-ratios, two-sided menus become multi-sided menus). The binary exposition conveys the essential ideas with lighter notation, and it is also the setting that our empirical application requires.

We bring the framework to a large-scale application in risky choice. We study the `choices13k` dataset of Peterson et al. (2021), which contains thousands of distinct binary lottery menus with repeated observations per menu, so that each menu can be summarized by a stable choice frequency. This setting is ideal for our purpose: the environment space is rich, predictive accuracy is a meaningful benchmark, and the structure of the mapping from menus to behavior is precisely the object of interest.

We construct a small library of parameter-free decision rules spanning canonical behavioral mechanisms studied in the literature - extreme-outcome screening, modal-outcome comparisons, salience-based comparisons, regret- and disappointment-type comparisons, and limited-consideration-style defaults - and impose an activity discipline under which a rule can influence predicted behavior only when it delivers a decisive recommendation. We estimate a differentiable gate that maps observable menu features into propensities over rules, and we evaluate all models out of sample using the same cross-validation protocol as Peterson et al. (2021). We then use the fitted mixture representation to report rule-level diagnostics (responsibility weights, concentration, and refit-based ablations) and to study how inferred rule responsibility shifts systematically with interpretable menu primitives such as tradeoff complexity and dispersion asymmetry. Finally, we compute and report identification diagnostics for the fitted gate, documenting when and how the procedural decomposition is empirically pinned down on the realized support of menus.

We find that rule-gating delivers large predictive gains relative to structured benchmarks while remaining more disciplined than the most flexible architectures. In out-of-sample evaluation on `choices13k`, rule-gating (MSE 0.0128) substantially outperforms Neural EU (0.0222), Neural CPT (0.0215), Neural PT (0.0206), and the value-based network (0.0192), and outperforms the context-

dependent model (0.0134), with only MOT (0.0114) achieving lower MSE. Using Neural EU as the baseline and MOT as the flexible benchmark, rule-gating closes about 87% of the baseline-to-MOT gap, compared to $\approx 28\%$ for the value-based model and 7%–15% for the prospect-theoretic benchmarks. Under permutation-fit restrictiveness, rule-gating and the structured benchmarks are essentially fully restrictive (near 100%), whereas MOT is markedly less so ($\approx 20\%$), indicating that rule-gating’s high completeness does not come from generic capacity. Portability reinforces this: when exported to CPC18 (Erev et al., 2017; Plonsky et al., 2017) without re-tuning, rule-gating and the context-dependent model transfer well (CPC18 MSE 0.0170 vs. 0.0172; trial-level Brier 0.197 vs. 0.198), far ahead of the structured benchmarks (≈ 0.032), while MOT deteriorates sharply (0.0926).

A central advantage of the RRM is that it does not deliver predictions as an opaque function of menu features. For each menu, the model determines which rules are *active*—which procedures induce a strict FOSD ranking—and distributes weight across active rules, producing an explicit mixture of rule-generated recommendations. This structure lets us translate predictive performance into interpretable objects: average effective responsibility of each procedure, concentration of the fitted mixture, and refit-based ablations that isolate which procedures are pivotal for prediction.

We find that effective responsibility is concentrated on a small set of psychologically standard procedures: extreme-outcome screening, modal-outcome comparisons, and salience-based comparisons carry the largest non-attention shares. Ablations are even more selective: removing either salience-based comparison produces the largest deterioration, followed by extreme-max and security-type screening, whereas modal-outcome, regret-, and disappointment-type procedures contribute little incremental content. Rule responsibility shifts systematically with objective menu primitives: along tradeoff complexity, the mixture reallocates toward attention and extreme-outcome screening and away from modal-outcome comparisons; along dispersion asymmetry, the pattern reverses on key dimensions.

We subject the framework to a battery of robustness checks addressing identification, library composition, the attention channel, the activity discipline, and the choice of gate features. The identification diagnostics confirm that both conditions of the global identification theorem are satisfied on the Choices13k data, with rule rankings by w_f and $\phi(f)$ highly stable across training samples. Cross-fitted library selection retains the bulk of accuracy with $k = 7$ rules, and the selected rules coincide with those receiving the highest responsibility weights. Removing the two attention rules brings MSE to 0.0201, still outperforming most structured benchmarks. Varying the activity discipline reveals that over-restricting the activity set is more costly than removing it, so the FOSD-based activation is best understood as an *interpretive* discipline rather than a predictive one. A placebo test confirms that the rule indicators carry genuine predictive content, rule-gating outperforms standard classifiers on rule features, and the interpretable gate features $z(A)$ match or improve on the raw 40-dimensional encoding.

Our approach relates to the literatures on stochastic choice and limited attention or consideration. In random utility models (RUM), choice probabilities are generated by heterogeneity in latent utilities (McFadden, 2006; McFadden and Richter, 1991; Kitamura and Stoye, 2018). A large related literature builds on this framework to account for limited, random, or menu-dependent consideration, jointly recovering preferences and attention/consideration mechanisms from stochastic choice data (Manzini and Mariotti, 2014; Cattaneo et al., 2020; Aguiar et al., 2023). The Random Rule Model (RRM) adopts a different primitive: stochasticity operates through randomization over a small library of interpretable decision procedures rather than through random utilities or random consideration sets. Moreover, the set of procedures that can influence a given menu is disciplined

menu-by-menu by an explicit dominance-based activity criterion. The RRM should therefore be viewed as a procedural stochastic-choice model: it provides a complementary, mechanism-oriented description of the choice process that is generally neither nested nor nests, the RUM and attention models.

On the behavioral side, our work complements the literature that explains choice anomalies through menu-dependent perception and evaluation (probability weighting, reference dependence, salience, regret and disappointment, and limited attention; see, e.g., Kahneman and Tversky, 1979; Tversky and Kahneman, 1992; Prelec, 1998; Kőszegi and Rabin, 2006; Bordalo et al., 2012; Loomes and Sugden, 1986; Bell, 1985; Gul, 1991; Masatlioglu et al., 2012; Manzini and Mariotti, 2014). It also connects to the broader tradition of modeling choice as the outcome of procedures and rules under bounded rationality and simplicity constraints (Simon, 1955; Tversky and Kahneman, 1974; Kahneman et al., 1982; Rubinstein, 1988; Aumann, 2008, 2019; Manzini and Mariotti, 2007, 2012; Cherepanov et al., 2013; Rubinstein and Salant, 2006; Salant and Rubinstein, 2008, 2011). Relative to this literature, our contribution is methodological: we provide a scalable estimation strategy for menu-dependent random switching among simple procedures, and we show how to map predictive performance into procedure-level implications in a large dataset.

Our approach builds on the decision-rule framework in Seror (2026). That paper develops a library of decision rules for risky decisions, and introduces concentration and overlap diagnostics to study which rules can rationalize observed choices, without targeting predictive performance. The present paper repurposes the same core primitives to build a predictive Random Rule Model (RRM): behavior is generated by random switching among transparent decision procedures, conditional on which procedures are active on a given menu.

Our mechanism results also relate to the literature on complexity and rule selection (Arrieta and Nielsen, 2024; Halevy and Mayraz, 2024; Puri, 2025). Closest to our analysis, Enke and Shubbatt (2023) construct menu-based complexity indices and show that “tradeoff complexity” predicts behavioral signatures in large-scale choice data. We build on this by studying how complexity and dispersion asymmetry are associated with systematic reallocation of procedure weights inside an interpretable random-rule mixture.

Our approach also speaks to the recent agenda of empirical machine learning in economics (Liang, 2025). Our completeness normalization follows recent work benchmarking economic structure against flexible ML baselines (e.g., Peysakhovich and Naecker, 2017; Fudenberg and Liang, 2020; Fudenberg and Puri, 2022; Fudenberg et al., 2022); our restrictiveness diagnostic applies the logic of Fudenberg et al. (2026); and we implement a portability exercise targeting external validity. Finally, a growing literature documents strong out-of-sample performance in risky choice (e.g., Erev et al., 2010, 2017; Plonsky et al., 2016; Peterson et al., 2021). Our contribution is to show that a disciplined mixture of interpretable procedures can recover a large share of these predictive gains while producing mechanism-level objects that are directly interpretable in economic terms.

2 Model

We develop the model and the identification theory for binary lottery menus, which is the setting of our empirical application. Appendix A presents the fully general framework covering arbitrary menu sizes, general dominance preorders, and multinomial choice. The two treatments share the same structure - a grouped-softmax representation, activity-conditional normalization, and verifiable conditions for global identification - with the main difference being notational: log-odds become

log-ratios and two-sided menus become multi-sided menus. The binary exposition thus conveys the essential ideas with lighter notation.

2.1 Setup

A *menu* (choice set) is a binary set $A = \{L^1, L^2\}$ of lotteries, each lottery being a finite-support distribution over monetary outcomes. We label L^1 the left choice and L^2 the right choice. Let $\mathcal{A}_{\text{full}}$ denote the full set of menus in the dataset. Each $A \in \mathcal{A}_{\text{full}}$ is observed $n(A) \geq 1$ times. Let $x_m(A) \in \{L^1, L^2\}$ be the realized choice in repetition $m \in \{1, \dots, n(A)\}$.¹ The menu-level left-choice frequency is

$$\hat{p}(A) := \frac{1}{n(A)} \sum_{m=1}^{n(A)} \mathbf{1}\{x_m(A) = L^1\} \in [0, 1].$$

We interpret $\hat{p}(A)$ as estimating a population choice probability $p(A) := \mathbb{P}(L^1 \mid A)$. A predictor is a function $g : \mathcal{A}_{\text{full}} \rightarrow [0, 1]$ intended to approximate $p(\cdot)$.

The dataset is a collection of observations $D = \{(x_t, A_t)\}_{t \in \mathcal{T}}$, where $\mathcal{T} := \{1, \dots, T\}$. The choice environment is characterized by the pair $((X, \succeq), \mathcal{A}_{\text{full}})$, where $\mathcal{A}_{\text{full}} = \{A_t\}_{t \in \mathcal{T}}$ and \succeq is a fixed dominance preorder on X . The statement $L^1 \succeq L^2$ means that L^1 is unambiguously perceived as better than L^2 according to the normative standard. We write \triangleright for the strict part of \succeq :

$$L^1 \triangleright L^2 \iff L^1 \succeq L^2 \text{ and not } (L^2 \succeq L^1).$$

We adopt First-Order Stochastic Dominance (FSD) as the dominance criterion.

Definition 1 (First-Order Stochastic Dominance). Let $L^1, L^2 \in X$. Let $\text{supp}(L^1) \cup \text{supp}(L^2) = \{z_1 < \dots < z_M\}$ be the ordered union of their supports. For $\ell \in \{1, 2\}$, let $\pi_k^\ell := \Pr_{L^\ell}(z_k)$ with the convention $\pi_k^\ell = 0$ when $z_k \notin \text{supp}(L^\ell)$, and define the right-tail cumulative sums $S_i^\ell := \sum_{k=i}^M \pi_k^\ell$, $i = 1, \dots, M$. We say that $L^1 \succeq_{\text{FSD}} L^2$ if and only if $S_i^1 \geq S_i^2$ for all $i = 1, \dots, M$. We denote the strict part by $>_{\text{FSD}}$.

Acts and States. For some of our decision rules introduced later, it is convenient to think of each lottery as induced by a state-contingent act. Formally, a choice problem can equivalently be described by a finite state space $S = \{1, \dots, n\}$, objective state probabilities $(p_s)_{s \in S}$, and, for each menu $A_t = \{L_t^1, L_t^2\}$, two acts corresponding to the two lotteries:

$$L_t^i \equiv (u_t^i(s))_{s \in S}, \quad u_t^i(s) \in \mathbb{R}.$$

Given $(p_s)_{s \in S}$, the act L_t^i induces a lottery representation $(z_t^i, \pi_t^i) \in X$ by grouping equal prizes and assigning to each distinct payoff its total probability:

$$\pi_{t,k}^i = \sum_{s \in S: u_t^i(s) = z_{t,k}^i} p_s.$$

The primitives of our model are lotteries, and all subsequent rules - including regret- and disappointment-type rules - are defined as functions of the lottery representation (or of a canonical state space constructed from the marginal distributions via the product measure over outcome pairs, as described in Section 4). Hence the lottery representation is without loss of generality for the properties we study. We will use the state-space view only when defining several rules, and otherwise work with the simpler lottery notation introduced above.

¹Within each menu we label options as “Left” (L^1) and “Right” (L^2) using the dataset’s fixed convention.

2.2 Rule library and rule-induced perceived lotteries

We model behavior as the outcome of a small library of simple decision rules. Each rule provides a clear-cut line of conduct: it extracts a coarse feature of the menu, converts each option into a (perceived) lottery - often a sure outcome in our implementation - and then recommends the option that is superior according to FSD. For example, the decision rule can be “choose the option with the better worst-case outcome”.

We follow Seror (2026) in the characterization of rules below. Let \mathcal{F} be a finite collection of rules. Each rule maps a binary menu to a perceived binary menu:

$$f : X \times X \rightarrow X \times X, \quad f(L^1, L^2) = (\pi_f(L^1; L^2), \pi_f(L^2; L^1)),$$

where $\pi_f(L^i; L^j) \in X$ is a finite-support lottery. The map π_f may depend only on the option being evaluated (lottery-specific rule) or also on the alternative (menu-dependent rule). We evaluate perceived lotteries using the same dominance preorder as for objective lotteries; throughout the paper, \succeq is First-Order Stochastic Dominance (FSD).

For each menu $A = \{L^1, L^2\}$ and each rule $f \in \mathcal{F}$, define the *activity* and *left-recommendation* indicators

$$A_f(A) := \mathbf{1}\left\{\pi_f(L^1; L^2) \succ_{\text{FSD}} \pi_f(L^2; L^1) \text{ or } \pi_f(L^2; L^1) \succ_{\text{FSD}} \pi_f(L^1; L^2)\right\}, \quad (1)$$

$$L_f(A) := \mathbf{1}\left\{\pi_f(L^1; L^2) \succ_{\text{FSD}} \pi_f(L^2; L^1)\right\}. \quad (2)$$

Thus $A_f(A) = 1$ means that rule f yields a *strict* dominance comparison in one direction (the rule is *decisive* at A), while $L_f(A) = 1$ means that, when decisive, it recommends choosing the left option.

Definition 2 (Activity). A rule $f \in \mathcal{F}$ is *active* at menu A if $A_f(A) = 1$, and *inactive* otherwise.

2.3 Conditional on Activity Random Rule Model (CA-RRM)

A Conditional on Activity Random Rule Model (CA-RRM) assigns to each menu A a vector $q(A) = \{q_f(A)\}_{f \in \mathcal{F}} \in \Delta^{F-1}$, where $q_f(A)$ is the propensity to apply rule f at A . Since not all rules are decisive at all menus, the model conditions on *activity*. We define the left mass and active mass:

$$\ell(A; q) = \sum_{f \in \mathcal{F}} q_f(A) L_f(A), \quad m(A; q) = \sum_{f \in \mathcal{F}} q_f(A) A_f(A).$$

The CA-RRM predicted left-choice probability is

$$g_{\text{CA}}(A) = \frac{\ell(A; q)}{\max\{m(A; q), m_{\min}\}} \in [0, 1], \quad (3)$$

where $m_{\min} > 0$ is a small guard constant to prevent numerical instability if the total active mass is near zero. In practice however, we have two “attention” rules in the library \mathcal{F} that can always be active, so $m(A; q)$ is typically strictly positive.

2.4 Rule-gating parameterization

CA-RRM becomes a *rule-gating predictor* when $q(A)$ is parameterized by a differentiable gate. Let $\psi(A) \in \mathbb{R}^d$ be a fixed-length encoding of the menu (defined precisely in Section 6.3). We use a softmax gate:

$$q_f(A; \theta) = \frac{\exp(\alpha_f + \beta_f^\top \psi(A))}{\sum_{g \in \mathcal{F}} \exp(\alpha_g + \beta_g^\top \psi(A))}, \quad (4)$$

where $\theta = \{(\alpha_f, \beta_f)\}_{f \in \mathcal{F}}$. The resulting predictor is $g_{\text{RG}}(A; \theta) = g_{\text{CA}}(A; q(\cdot; \theta))$ as in (3).

Combining (3) with (4), we have

$$g_{\text{RG}}(A; \theta) = \frac{\sum_{f \in \mathcal{F}} q_f(A; \theta) L_f(A)}{\sum_{f \in \mathcal{F}} q_f(A; \theta) A_f(A)} \quad (\text{up to the small guard } m_{\min}).$$

We define the *conditional-on-activity weights*

$$\tilde{q}_f(A; \theta) := \frac{q_f(A; \theta) A_f(A)}{\sum_{g \in \mathcal{F}} q_g(A; \theta) A_g(A)} \in [0, 1], \quad \sum_{f \in \mathcal{F}} \tilde{q}_f(A; \theta) = 1 \quad (5)$$

whenever the denominator is positive.² Then the CA-RRM prediction admits the simple mixture form

$$g_{\text{RG}}(A; \theta) = \sum_{f \in \mathcal{F}} \tilde{q}_f(A; \theta) L_f(A). \quad (6)$$

From (6), a CA-RRM operates as a mixture over deterministic rule recommendations, after filtering out rules that are inactive at A .

3 Identification via Rule Switching

This section clarifies when the gate parameters $\theta = \{(\alpha_f, \beta_f)\}_{f \in \mathcal{F}}$ are pinned down by menu-level choice frequencies. The key identifying force is *rule switching*: because different rules recommend different sides in different menus, the decisive-side pattern varies across the menu support, and this variation pins down the relative rule weights.

From CA-RRM to a collapsed binary logit index (identity, not a new model). For a menu $A = \{L^1, L^2\}$, define the decisive-left and decisive-right sets

$$\mathcal{I}_L(A) := \{f \in \mathcal{F} : A_f(A) = 1, L_f(A) = 1\}, \quad \mathcal{I}_R(A) := \{f \in \mathcal{F} : A_f(A) = 1, L_f(A) = 0\}.$$

Ignoring the numerical guard m_{\min} (inactive in our implementation), the softmax gate (4) combined with the CA normalization yields

$$g_{\text{RG}}(A; \theta) = \frac{\sum_{f \in \mathcal{I}_L(A)} \exp(\alpha_f + \beta_f^\top \psi(A))}{\sum_{f \in \mathcal{I}_L(A) \cup \mathcal{I}_R(A)} \exp(\alpha_f + \beta_f^\top \psi(A))}. \quad (7)$$

²In our implementation, rules A1 and A2 are always included and are decisive for essentially all menus, so the denominator is typically well away from zero.

Define the inclusive values

$$V_L(A; \theta) := \log \sum_{f \in \mathcal{I}_L(A)} \exp(\alpha_f + \beta_f^\top \psi(A)), \quad V_R(A; \theta) := \log \sum_{f \in \mathcal{I}_R(A)} \exp(\alpha_f + \beta_f^\top \psi(A)).$$

Whenever $\mathcal{I}_L(A)$ and $\mathcal{I}_R(A)$ are both nonempty,

$$\log \frac{g_{\text{RG}}(A; \theta)}{1 - g_{\text{RG}}(A; \theta)} = V_L(A; \theta) - V_R(A; \theta). \quad (8)$$

Observed object. Let $\mathcal{A}_2 := \{A \in \mathcal{A}_{\text{full}} : \mathcal{I}_L(A) \neq \emptyset, \mathcal{I}_R(A) \neq \emptyset\}$ denote the set of *two-sided* menus. For $A \in \mathcal{A}_2$, define the population log-odds

$$\delta(A) := \log \frac{p(A)}{1 - p(A)} = V_L(A; \theta) - V_R(A; \theta), \quad (9)$$

where $p(A) = \Pr(L^1 | A)$.

Normalization and parameter vector. Because the softmax gate is invariant to adding a common constant to all α_f and a common vector to all β_f , we impose a location normalization: fix one baseline rule $f_0 \in \mathcal{F}$ and set

$$(\alpha_{f_0}, \beta_{f_0}) = (0, 0). \quad (10)$$

Let $\vartheta \in \mathbb{R}^K$ collect the remaining free parameters, with $K = (|\mathcal{F}| - 1)(1 + \dim(\psi))$.

Decisive-side indicators and the H matrix. For each rule f and menu A , define the decisive-side indicators

$$\kappa_f^L(A) := \mathbf{1}\{f \in \mathcal{I}_L(A)\}, \quad \kappa_f^R(A) := \mathbf{1}\{f \in \mathcal{I}_R(A)\},$$

and write the odds ratio $r(A) := p(A)/(1 - p(A))$. For any $x \in \mathbb{R}^d$ define the positive weight vector $\omega_f(x) := \exp(\alpha_f + \beta_f^\top x)$. Cross-multiplying the odds form of the model yields, for each menu A with $\psi(A) = x$,

$$\sum_{f \in \mathcal{F}} (\kappa_f^L(A) - r(A)\kappa_f^R(A)) \omega_f(x) = 0, \quad (11)$$

i.e. $h(A)^\top \omega(x) = 0$ where $h_f(A) := \kappa_f^L(A) - r(A)\kappa_f^R(A)$.

Global identification theorem.

Theorem 1 (Global identification under within-feature activity variation). *Consider the CA-RRM with affine indices $s_f(A) = \alpha_f + \beta_f^\top \psi(A)$, $f \in \mathcal{F}$. Assume $p(A) \in (0, 1)$ for all menus in the support, and impose the normalization $(\alpha_{f_0}, \beta_{f_0}) = (0, 0)$. Let $d = \dim(\psi)$. Suppose there exist $(d+1)$ feature values $x^{(0)}, \dots, x^{(d)}$ such that:*

(G1) **Within-feature variation in decisive-side patterns:** *For each $k \in \{0, \dots, d\}$, there exist $M_k \geq |\mathcal{F}| - 1$ menus A_{k1}, \dots, A_{kM_k} with $\psi(A_{km}) = x^{(k)}$ for all m , and the $M_k \times |\mathcal{F}|$ matrix*

$$H^{(k)} := \begin{pmatrix} h(A_{k1})^\top \\ \vdots \\ h(A_{kM_k})^\top \end{pmatrix}$$

has rank $|\mathcal{F}| - 1$.

(G2) **Affine richness of feature values:** The $(d+1) \times (d+1)$ matrix $X := \begin{pmatrix} 1 & (x^{(0)})^\top \\ \vdots & \vdots \\ 1 & (x^{(d)})^\top \end{pmatrix}$ has full rank.

Then the full parameter vector $\{(\alpha_f, \beta_f)\}_{f \in \mathcal{F}}$ is globally identified from the population objects $\{p(A), \kappa^L(A), \kappa^R(A), \psi(A)\}$, up to the normalization.

The proof, given in Appendix B, has two layers. The first layer identifies, at a fixed feature value x , the vector of relative rule weights $\omega(x) = (\exp(\alpha_f + \beta_f^\top x))_{f \in \mathcal{F}}$. For any menu A with $\psi(A) = x$, the model says that the odds of choosing left equal the ratio of total weight on rules decisive for left to total weight on rules decisive for right. Cross-multiplying turns this odds identity into a *linear* equation in the unknown weights $\omega(x)$, with coefficients determined by the decisive-side indicators $(\kappa^L(A), \kappa^R(A))$ and the observed odds $r(A)$. If we see many menus that share the same feature value x but exhibit different decisive-side patterns (because different rules switch sides across those menus), we obtain many independent linear equations for the *same* unknown vector $\omega(x)$. Condition (G1) requires that these equations be sufficiently rich - rank $|\mathcal{F}| - 1$ - so they pin down the relative weights of all rules at x (the remaining one degree of freedom is an overall scale). The CA location normalization then fixes that scale because it anchors one rule's weight at $\omega_{f_0}(x) \equiv 1$, yielding a unique $\omega(x)$ at each identifying feature value. The second layer then recovers the gate parameters. Once the weights are known at $(d+1)$ feature values, each rule f satisfies the linear relation $\log \omega_f(x^{(k)}) = \alpha_f + \beta_f^\top x^{(k)}$ across k . Condition (G2) (affine independence) ensures that the resulting $(d+1) \times (d+1)$ regressor matrix is invertible, so these $(d+1)$ equations uniquely solve for (α_f, β_f) rule-by-rule. In short: (G1) uses rule switching at fixed x to identify weights, and (G2) uses variation in x to map those weights back to the affine indices globally, rather than only locally.

Effective dimension. When the feature vector has structural redundancies (e.g., exact linear dependencies among coordinates), the theorem applies with d replaced by the effective dimension $d_{\text{eff}} := \text{rank}([\mathbf{1}, z]) - 1$, and identification holds for the gate parameters projected onto the effective feature subspace (i.e., up to the null space of $[\mathbf{1}, z]$). In practice, one can reparameterize the gate in terms of a d_{eff} -dimensional basis of the column space of $[\mathbf{1}, z]$, and identification then holds for the parameters associated with this effective feature space. In our application, the baseline gate features $z(A) \in \mathbb{R}^{12}$ have $d_{\text{eff}} = 11$ (the expected-value gap is a linear combination of the two level expected values).

Menu encoding. The feature vector $\psi(A) \in \mathbb{R}^{4M}$ is the fixed-length concatenation of sorted outcomes and probabilities for the two lotteries (Section 6.3 gives the precise definition).

Diagnostics: empirically assessing identification strength

Theorem 1 reduces identification to two verifiable conditions on the observed menu support. We report three diagnostics.

D1 (Two-sidedness). Report the fraction of menus that are two-sided: $\widehat{\text{Pr}}(A \in \mathcal{A}_2)$. This ensures the log-odds representation (9) is empirically meaningful.

D2 (Coverage and side-variation by rule). For each rule f , report (i) decisiveness frequency $\widehat{\Pr}(A_f(A) = 1)$ and (ii) side-variation conditional on decisiveness:

$$\widehat{\Pr}(f \in \mathcal{I}_L(A) \mid A_f(A) = 1), \quad \widehat{\Pr}(f \in \mathcal{I}_R(A) \mid A_f(A) = 1).$$

Rules that take both sides contribute sign-varying rows to the $H^{(k)}$ matrices, supporting condition (G1).

D3 (Verification of (G1) and (G2)). The diagnostic is implemented on the interpretable gate features $z(A) \in \mathbb{R}^{12}$ used in the baseline specification (Section 6.6). To check (G1), group menus into cells that share the same (or nearby) value of $z(A)$, and compute $\text{rank}(H^{(k)})$ for each cell via SVD. Condition (G1) is supported if at least $d_{\text{eff}} + 1$ cells achieve $\text{rank} \mid \mathcal{F} \mid - 1$, where d_{eff} is the effective dimension of the gate feature space. Among the cells satisfying (G1), check that their representative feature values span $\mathbb{R}^{d_{\text{eff}}}$ affinely; (G2) is supported if this affine rank condition holds.

Checking (G1) in practice. Because the gate features $z(A)$ are 12-dimensional summary statistics, many distinct menus share the same (or very close) feature value. We group menus into cells \mathcal{C}_k using exact equality of $z(A)$ where possible, supplemented by k -means clustering as a finite-sample heuristic. We retain cells with at least $\mid \mathcal{F} \mid - 1$ menus. For each cell, we form the matrix $\hat{H}^{(k)}$ by stacking the row vectors $\hat{h}(A)^\top = (\kappa_f^L(A) - \hat{r}(A)\kappa_f^R(A))_{f \in \mathcal{F}}$ over its menus (trimming $\hat{p}(A)$ to $[\varepsilon, 1 - \varepsilon]$ for numerical stability), and compute its numerical rank via SVD with a tolerance-based criterion. Assumption (G1) is supported if at least $d_{\text{eff}} + 1$ cells achieve $\text{rank}(\hat{H}^{(k)}) = \mid \mathcal{F} \mid - 1$. To verify (G2), we check that the centroids of cells satisfying (G1) are affinely independent.

If ψ is essentially injective (as with the raw 40-dimensional menu encoding), the sufficient global identification condition (G1) is not applicable, since no feature value is shared by multiple distinct menus. For completeness, Appendix O provides a local identification argument based on the Jacobian rank that does not require within-feature replication.

D1–D2 document that the model generates informative variation in left/right decisive sets. D3 provides empirical support for the sufficient conditions of Theorem 1 under the baseline gate specification with $z(A)$. We report the empirical results of these diagnostics on the Choices13k dataset in Section 9.1.

4 Rule library

The library described below is deliberately small and simple. Each element is a parameter-free heuristic that can be stated as a single line of conduct, implemented deterministically menu-by-menu, and produces a strict recommendation whenever it yields an unambiguous dominance comparison. Rather than postulating a global valuation model and fitting preference parameters, we treat behavior as switching among a few coarse procedures.

Notation. Let $\text{Supp}(L)$ be its finite support and let $x_{\min}(L) := \min \text{Supp}(L)$, $x_{\max}(L) := \max \text{Supp}(L)$. Write $\delta(z)$ for the degenerate lottery yielding z with probability one. Given outcomes $x, y \in \mathbb{R}$, define the (normalized) contrast

$$\text{contr}(x, y) := \frac{\mid x - y \mid}{\mid x \mid + \mid y \mid + 1}. \quad (12)$$

The outcomes x, y enter in their raw units (before the outcome rescaling applied to neural network features in Section 6.3). The constant $+1$ in the denominator is a fixed regularization choice (not a tunable parameter) that prevents division by zero and pins down the scale in the raw-outcome units of the dataset. Because the contrast is not homogeneous of degree zero, the effective rule recommendations depend on the outcome scale of the data. The rules remain parameter-free in the sense that no parameter is estimated from data, but they are not invariant to affine transformations of outcomes; applying the same rules to payoffs denominated in cents rather than dollars could change which rules are active on some menus. This scale dependence is a limitation of the current formulation. For some rules we use a small set of *extreme pairings*. For $A = \{L^1, L^2\}$ define

$$\mathcal{P}(A) := \{(a, b) : a \in \{x_{\min}(L^1), x_{\max}(L^1)\}, b \in \{x_{\min}(L^2), x_{\max}(L^2)\}\},$$

which contains at most four outcome pairs.

Outcome simplification rules (MMn, MMa, MMx, MAP). These rules reduce each lottery to a single representative payoff (hence to a degenerate perceived lottery).

- MMN (security): “choose the option with the better worst-case outcome.”

$$\pi_{\text{MMN}}(L^i; L^j) := \delta(x_{\min}(L^i)).$$

- MMX (aspiration): “choose the option with the better best-case outcome.”

$$\pi_{\text{MMX}}(L^i; L^j) := \delta(x_{\max}(L^i)).$$

- MMA (midrange focus): “choose based on the midpoint between best and worst outcomes.”

$$\pi_{\text{MMA}}(L^i; L^j) := \delta\left(\frac{1}{2}(x_{\min}(L^i) + x_{\max}(L^i))\right).$$

- MAP (most-likely outcome): “choose the option whose most likely outcome is higher.” Let $z_{\text{mode}}(L)$ be the (highest) modal payoff of L (ties broken upward), then

$$\pi_{\text{MAP}}(L^i; L^j) := \delta(z_{\text{mode}}(L^i)).$$

Salience rules (SAL, SAL2). These rules formalize “attention to what stands out.” They compare the options using one salient extreme pairing. Let $\mathcal{P}(A) = \{(a_k, b_k)\}_{k=1}^4$ and define salience scores $c_k := \text{contr}(a_k, b_k)$.

- SAL (most salient comparison): “choose according to the single most salient extreme comparison.” Let $k^* \in \arg \max_k c_k$ (ties broken deterministically). Define

$$\pi_{\text{SAL}}(L^1; L^2) := \delta(a_{k^*}), \quad \pi_{\text{SAL}}(L^2; L^1) := \delta(b_{k^*}).$$

- SAL2 (second-most salient comparison): “choose according to the second most salient extreme comparison.” Let $c_{(1)} \geq c_{(2)}$ denote the two largest values among $\{c_k\}_{k=1}^4$ and let $k^{(2)}$ be an index attaining $c_{(2)}$. When $c_{(1)} = c_{(2)}$ the rule is left inactive (no well-defined “second” salient comparison); otherwise set

$$\pi_{\text{SAL2}}(L^1; L^2) := \delta(a_{k^{(2)}}), \quad \pi_{\text{SAL2}}(L^2; L^1) := \delta(b_{k^{(2)}}).$$

Regret rules (REG, REGmed). Following Loomes and Sugden (1982), these rules define the state space as the set of all outcome pairs (x_i, y_j) with $x_i \in \text{Supp}(L^1)$, $y_j \in \text{Supp}(L^2)$, each occurring with probability $p_i^{L^1} \cdot p_j^{L^2}$. In state (i, j) , the regret of choosing L^1 is $d_{ij}^L := [y_j - x_i]_+$ and the regret of choosing L^2 is $d_{ij}^R := [x_i - y_j]_+$.

- REG (regret-distribution dominance): “choose the option whose negated-regret distribution first-order stochastically dominates.” The perceived lottery for L^1 given L^2 is the full negated-regret distribution (i.e., the distribution of $-d_{ij}^L$, so that “larger is better” under the usual FSD convention)

$$\pi_{\text{REG}}(L^1; L^2) := \sum_{i,j} p_i^{L^1} p_j^{L^2} \delta(-d_{ij}^L), \quad \pi_{\text{REG}}(L^2; L^1) := \sum_{i,j} p_i^{L^1} p_j^{L^2} \delta(-d_{ij}^R).$$

The rule is active when one negated-regret distribution strictly first-order stochastically dominates the other.

- REGMED (median regret): “choose the option with the smaller probability-weighted median regret.”

$$R_{\text{med}}^L := \text{wmed}(\{d_{ij}^L\}, \{p_i^{L^1} p_j^{L^2}\}), \quad R_{\text{med}}^R := \text{wmed}(\{d_{ij}^R\}, \{p_i^{L^1} p_j^{L^2}\}),$$

where wmed denotes the weighted median; then $\pi_{\text{REGMED}}(L^1; L^2) := \delta(-R_{\text{med}}^L)$ and $\pi_{\text{REGMED}}(L^2; L^1) := \delta(-R_{\text{med}}^R)$.

Disappointment rules (DIS, DISmed). These rules treat the most likely outcome as a reference point and penalize downside contrasts below it. For a lottery L , let $z_{\text{mode}}(L)$ be its (highest) modal payoff, and define the set of downside payoffs $Z^-(L) := \{z \in \text{Supp}(L) : z < z_{\text{mode}}(L)\}$. Define the disappointment contrasts $s(z) := \text{contr}(z_{\text{mode}}(L), z)$ for $z \in Z^-(L)$ (and set the index to 0 if $Z^-(L) = \emptyset$).

- DIS (worst-case disappointment): “avoid the option with the largest downside contrast below its most likely outcome.”

$$D(L) := \max_{z \in Z^-(L)} s(z) \quad (\text{with } D(L) = 0 \text{ if } Z^-(L) = \emptyset), \quad \pi_{\text{DIS}}(L^i; L^j) := \delta(-D(L^i)).$$

- DISMED (typical downside disappointment): “avoid the option with the second-largest downside contrast below its most likely outcome.” If $|Z^-(L)| \geq 2$, let $s_{(1)} \geq s_{(2)} \geq \dots$ be the sorted contrasts and set $D_{\text{med}}(L) := s_{(2)}$; otherwise set $D_{\text{med}}(L) := D(L)$. Then

$$\pi_{\text{DISMED}}(L^i; L^j) := \delta(-D_{\text{med}}(L^i)).$$

Extreme attention rules (A1, A2). The last group encodes extreme one-sided consideration sets. Fix $M > 0$ so that $-M$ lies strictly below all payoffs in the dataset.

- A1 (attention to L^1): “treat the right option as an extremely bad sure outcome.”

$$\pi_{\text{A1}}(L^1; L^2) = L^1, \quad \pi_{\text{A1}}(L^2; L^1) = \delta(-M).$$

- A2 (attention to L^2): symmetric.

$$\pi_{\text{A2}}(L^1; L^2) = \delta(-M), \quad \pi_{\text{A2}}(L^2; L^1) = L^2.$$

In our implementation, both A1 and A2 are always included; they also ensure that at least one rule is decisive at essentially every menu, which stabilizes the CA-RRM normalization in (3).

Discussion

The library spans five broad mechanisms emphasized in behavioral and bounded-rationality work—outcome simplification, salience-driven attention, regret, disappointment, and limited consideration—implemented here in a deliberately coarse, parameter-free form. The gate does not estimate a valuation model; it learns *when* each simple line of conduct best predicts behavior.

Within-family variants and why we avoid “aggregate” rules. Several rules are variants within a common mechanism (e.g. SAL vs. SAL2, REG vs. REGMED). When two variants are active at the same menu, the conditional-on-activity weights (5) yield a direct within-family split. A natural alternative would be a single “aggregate” rule that combines information across all ranks, but such a rule requires specifying how ranks are weighted—absent preference parameters there is no canonical choice. We instead use discrete variants (top-ranked vs. second-ranked comparison) that probe sensitivity to the ranking without introducing an explicit aggregation scheme, stopping at rank two to keep the library small.

4.1 Rule-level Diagnostics

The rule-gating predictor is transparent at the menu level: by (6), each predicted choice probability is a convex combination of deterministic rule recommendations, with weights $\tilde{q}_f(A; \hat{\theta})$ that can be interpreted as *conditional-on-activity responsibilities*. This section introduces summary diagnostics that turn these menu-by-menu decompositions into interpretable *rule-level* statements. The goal is twofold: (i) quantify which procedures the fitted gate actually uses on average, and (ii) distinguish rules that are *essential for fit* from rules that mainly act as substitutes.

Effective responsibility weights and concentration

Because the CA-RRM conditions on activity, the economically meaningful notion of “rule usage” is the gate mass *among decisive rules*. For each menu A_t and each rule f , define the effective responsibility

$$\tilde{q}_{tf} := \tilde{q}_f(A_t; \hat{\theta}) = \frac{q_f(A_t; \hat{\theta}) A_f(A_t)}{\sum_{g \in \mathcal{F}} q_g(A_t; \hat{\theta}) A_g(A_t)}, \quad (13)$$

whenever the denominator is positive.³ The *effective responsibility weight* of rule f is the average responsibility across menus,

$$w_f := \frac{1}{N} \sum_{i=1}^N \tilde{q}_{if}, \quad \sum_{f \in \mathcal{F}} w_f = 1. \quad (14)$$

Thus w_f measures the average share of decision mass attributed to rule f , *conditional on the rule being eligible to speak* (i.e., active) at each menu.

³In our implementation, the two attention rules A1 and A2 are always included and are decisive for essentially all menus, so the denominator is typically well away from zero.

Rule Concentration

To summarize whether the fitted mixture concentrates on a few procedures or is diffuse across many, we report the Herfindahl concentration of responsibility weights,

$$\text{HHI}(F) := \sum_{f \in \mathcal{F}} w_f^2. \quad (15)$$

Higher $\text{HHI}(F)$ indicates that a small subset of rules accounts for most effective responsibility, whereas lower $\text{HHI}(F)$ indicates a more even allocation across rules. This statistic is informative because the rule-gating predictor is interpretable only to the extent that its effective responsibilities are *parsimonious*: a high concentration means that most menus are explained by a small repertoire of named procedures, while a low concentration suggests that predictive success relies on a broad set of substitutes. We also report the *effective number of rules*

$$N_{\text{eff}}(F) := \frac{1}{\text{HHI}(F)} \in [1, |\mathcal{F}|],$$

which can be read as the number of equally-weighted rules that would generate the same concentration. For example, $N_{\text{eff}} = 3$ means that the fitted model is about as concentrated as one that splits effective responsibility evenly across three procedures. We use $\text{HHI}(F)$ (and N_{eff}) as a compact summary of whether the fitted rule-gating model achieves accuracy through a few unifying mechanisms or through a diffuse patchwork of rules.

Predictive ablation index $\phi(f)$

Responsibility weights are descriptive, but they do not by themselves tell whether a rule is *necessary* for predictive accuracy: a rule can carry substantial mass yet be redundant because other rules typically make the same recommendation, and conversely a rarely-used rule can matter sharply in a small region of menu space. To quantify importance for fit, we use a refit-and-compare ablation diagnostic.

For each rule $f \in \mathcal{F} \setminus \{A1, A2\}$, let MSE^{-f} denote the cross-validated test MSE of rule-gating when f is removed from the library and the gate is retrained on the remaining rules. Let MSE^{full} be the corresponding MSE for the full library. Define

$$\phi(f) := \frac{\text{MSE}^{-f} - \text{MSE}^{\text{full}}}{\text{MSE}^{\text{full}}}. \quad (16)$$

Thus $\phi(f) > 0$ means that removing f worsens out-of-sample accuracy, and larger values indicate a more prediction-critical procedure.⁴

Concentration impact $\sigma_N(f)$

Finally, we ask whether a rule acts as a *unifier* (its presence makes effective responsibility concentrate on a small repertoire of procedures) or instead as a *substitute* that helps spread responsibility across the library. For each $f \in \mathcal{F} \setminus \{A1, A2\}$, we refit the gate after removing f and recompute the

⁴We exclude A1/A2 from ablation because they serve as stability anchors by ensuring decisiveness at essentially every menu; dropping them would confound behavioral importance with numerical degeneracy of the CA-RRM normalization.

effective responsibility weights and concentration. Let HHI^{-f} denote the resulting concentration, and let $N_{\text{eff}}^{-f} := 1/\text{HHI}^{-f}$ be the associated effective number of rules (recall $N_{\text{eff}}(F) = 1/\text{HHI}(F)$ from above). We summarize the *concentration impact* of rule f by the relative change in the effective number of rules:

$$\sigma_N(f) := \frac{N_{\text{eff}}^{-f} - N_{\text{eff}}(F)}{N_{\text{eff}}(F)}. \quad (17)$$

Thus $\sigma_N(f) > 0$ means that removing f increases the effective number of rules (the fitted mixture becomes more diffuse). Conversely, $\sigma_N(f) < 0$ means that removing f decreases the effective number of rules (the mixture becomes more concentrated), so f primarily acts as a substitute/diversifier: when it is unavailable, the gate reallocates mass more sharply onto a smaller set of remaining procedures. This refit-based diagnostic complements the ablation index $\phi(f)$: $\phi(f)$ measures the *predictive* importance of f , while $\sigma_N(f)$ measures its role in shaping the *structure* of the fitted mixture. Importantly, $\sigma_N(f)$ is computed after a full refit and therefore reflects equilibrium reallocation of responsibility.

The pair $(\phi(f), \sigma_N(f))$ separates distinct roles. A large $\phi(f)$ indicates that the procedure improves predictive fit and is not easily replaced by the rest of the library; the sign and magnitude of $\sigma_N(f)$ indicate whether that procedure also shapes the overall mixture structure (concentrating or diversifying effective responsibility). In the Results section we report $(w_f, \phi(f), \sigma_N(f))$ side-by-side to identify rules that are heavily used, rules that are essential for accuracy, and rules that mainly act as substitutes or robustness variants.

5 Benchmark models

We benchmark rule-gating against the main differentiable model classes studied by Peterson et al. (2021). For most benchmark classes, a model first assigns each gamble a value $V(\cdot)$ and then maps values into a choice probability via a logit (softmax) link:

$$\hat{p}(A) = \frac{\exp(\eta V(L^1))}{\exp(\eta V(L^1)) + \exp(\eta V(L^2))}, \quad (18)$$

where η is a free “determinism” (inverse-noise) parameter. The exception is the fully context-dependent network, which directly outputs $\hat{p}(A)$.

Neural EU. This class retains the expected-utility structure $V(L) = \sum_k p_k u(x_k)$ but learns the utility function $u(\cdot)$ as a small neural network, jointly with η .

Neural PT. This class retains the prospect-theory structure $V(L) = \sum_k u(x_k) \pi(p_k)$ but learns both $u(\cdot)$ and $\pi(\cdot)$ as neural networks, jointly with η .

Neural CPT. This class implements cumulative prospect theory with separate probability-weighting functions for gains and losses, applied cumulatively to ordered outcomes. The functions $u(\cdot)$ and $\pi^+(\cdot), \pi^-(\cdot)$ are learned by neural networks, jointly with η .

Value-Based. This class relaxes the linear aggregation of outcomes and probabilities within each gamble while still valuing gambles independently:

$$V(L) = f(x^L, p^L),$$

where f is a neural network taking the padded outcome and probability vectors as input; choice probabilities follow (18).

Context-Dependent. This is the most flexible differentiable benchmark: a neural network directly maps the full description of both gambles to a choice probability,

$$\hat{p}(A) = g(x^{L^1}, p^{L^1}, x^{L^2}, p^{L^2}),$$

without imposing a representation in terms of separate values $V(L^1), V(L^2)$.

Mixture of Theories (MOT). MOT is a structured context-dependent benchmark in which the model selects (softly) among a small set of subjective utility functions and probability-weighting functions using gating networks (a mixture-of-experts architecture) (Peterson et al., 2021, Supplementary Materials). Separate softmax gates output mixture weights for utilities and for probability weighting; values are computed by mixing two candidate utility functions and two candidate probability-weighting functions, and then mapped into a choice probability via (18). A separate component handles dominated gambles via an additional parameter (a fixed predicted probability for dominated choices).

6 Empirical design

This section explains what is being predicted, how menus are encoded, how each model is trained. The core object is the menu-level choice probability $p(A) = \Pr(L^1 | A)$; every model outputs a prediction $g(A) \in [0, 1]$ that we evaluate out of sample.

6.1 Dataset and target variable

We use the `choices13k` dataset introduced by Peterson et al. (2021), containing 13,006 binary risky-choice problems. Each problem corresponds to a menu $A = \{L^1, L^2\}$ and is repeated across many observations, allowing the computation of a menu-level choice frequency. We work with the filtered dataset that (i) removes ambiguous problems (masked probabilities) and (ii) keeps only problems for which feedback was provided, yielding $N = 9,831$ menus. The feedback restriction follows the baseline protocol of Peterson et al. (2021) and has a practical justification: feedback problems have more repetitions per menu, producing more precise estimates of the choice frequency $\hat{p}(A)$ that serves as our prediction target. Because our model is static (it maps menu features to a predicted choice probability without using feedback information), the feedback condition affects only the precision of the dependent variable, not the model’s information set.⁵ For each menu A , the dataset reports the fraction of times the left option is chosen. We denote this empirical frequency by $\hat{p}(A)$ and treat it as the target to be predicted.

⁵Feedback can in principle induce learning effects. If such dynamics are present, our static model captures the average behavior under the feedback regime.

6.2 Evaluation metric

Our main performance metric is the mean squared error (MSE):

$$\text{MSE}(g) = \frac{1}{T} \sum_{t=1}^T \left(g(A_t) - \hat{p}(A_t) \right)^2, \quad (19)$$

for $\{A_t\}_{t \in \{1, \dots, T\}} \subseteq \mathcal{A}_{\text{full}}$. The MSE is a scoring rule: it rewards probabilistic accuracy and penalizes both systematic bias and overconfidence. We focus on MSE because it is standard and is the primary metric reported by Peterson et al. (2021).

Because the number of trials n_t behind each menu-level frequency $\hat{p}(A_t)$ varies across menus, we also report a trial-weighted variant:

$$\text{MSE}_w(g) = \frac{\sum_{t=1}^T n_t \left(g(A_t) - \hat{p}(A_t) \right)^2}{\sum_{t=1}^T n_t}. \quad (20)$$

This metric downweights menus estimated from few trials, where $\hat{p}(A_t)$ is noisier, and gives a more precision-aware summary of predictive accuracy. We use the unweighted MSE as the primary metric for comparability with Peterson et al. (2021) and report MSE_w as a robustness check.

We also conduct paired split-level comparisons: for each pair of models, we compute per-fold metric differences and report their mean and standard error across the 50 splits (Appendix Table A.2).

Target variable as estimate. The menu-level choice frequency $\hat{p}(A)$ is itself an estimate of $p(A)$, computed from a finite number of trials $n(A)$. We treat $\hat{p}(A)$ as the prediction target without modeling the sampling process. This is appropriate because Choices13k menus typically aggregate many repetitions (median above 25). The trial-weighted metric MSE_w provides a precision-aware robustness check, and rankings are preserved (Table 1). The fold-level variability bands measure instability from random train/test partitions (the design component), not sampling variability in the choice frequencies; the design component dominates in our setting.

6.3 Menu encoding

All models take as input a fixed-length numerical encoding of the two lotteries in the menu. To align with Peterson et al. (2021), each lottery is represented by its list of outcomes and probabilities after sorting outcomes in increasing order, truncating to a maximum support size M and padding with zeros. We set $M = 10$ throughout.

Formally, for each lottery L with support points $\{(x_k, \pi_k)\}_{k=1}^K$, order outcomes so that $x_1 \leq \dots \leq x_K$ and define

$$x_{1:M}(L) = (x_1, \dots, x_{\min\{K, M\}}, 0, \dots, 0), \quad \pi_{1:M}(L) = (\pi_1, \dots, \pi_{\min\{K, M\}}, 0, \dots, 0).$$

The menu encoding is the concatenation

$$\psi(A) = \left(x_{1:M}(L^1), \pi_{1:M}(L^1), x_{1:M}(L^2), \pi_{1:M}(L^2) \right) \in \mathbb{R}^{4M}. \quad (21)$$

To stabilize optimization across models, we rescale outcomes by the maximum absolute payoff observed in the filtered sample; the same scaling is applied for all models and all folds. This

rescaling enters only the menu encoding $\psi(A)$ (and hence the gate features $z(A)$) used as inputs to differentiable models; it does not affect the rule indicators, which are computed on raw outcomes before any rescaling. The scaling is a fixed, data-wide preprocessing step applied identically to all models and folds.

6.4 Cross-validation protocol

We compare models using the out-of-sample evaluation structure of Peterson et al. (2021). The unit of observation for prediction is the menu, not the individual trial. We repeatedly split the set of menus into training and test sets, fit model parameters on the training set, and evaluate MSE on the held-out test set.

Splits. We generate $K = 50$ independent random splits of the N menus into 90% training and 10% test, as in Peterson et al. (2021). Each model is trained from scratch on each split.

Learning-rate selection. Each differentiable model is trained by gradient descent (Adam). Following Peterson et al. (2021), we select the learning rate from a small grid. To avoid selecting the learning rate on the same data used to evaluate generalization (as in Peterson et al., 2021, who select on test MSE), we use a two-pass protocol within each split. In Pass A (validation), we further partition the training set into an 80% sub-training set and a 20% validation set, train the model on the sub-training set for each candidate learning rate, and record the validation MSE. In Pass B (test), we retrain the model on the *full* training set using each candidate learning rate and evaluate MSE on the held-out test set. The reported performance of a model is the average test MSE (from Pass B) across the 50 splits at the learning rate that achieves the lowest average validation MSE (from Pass A). This two-pass validation protocol applies to all models *except* the Mixture of Theories (MOT). MOT relies on the HURD library’s internal training/validation logic, which does not expose hooks for overriding the train/validation partition or for extracting per-menu predictions at the validation stage. We therefore select MOT’s learning rate by mean *test* MSE across splits, following Peterson et al. (2021). This asymmetry is conservative: it gives MOT the benefit of test-set-informed learning-rate selection, which, if anything, biases the comparison in MOT’s favor.

Implementation details. We adopt the same network sizes and training horizons used by Peterson et al. (2021) (and their Supplementary Materials) for Neural EU/PT/CPT, Value-Based, Context-Dependent, and MOT. We keep all such hyperparameters fixed across splits and do not tune architectures. The only tuned hyperparameter is the learning rate.

6.5 Estimation of the rule-gating model

The rule-gating model differs from the benchmark neural predictors in a key way: the *rules are deterministic and parameter-free*. Estimation concerns only the *gate*, i.e. the mapping from menu features $z(A)$ to rule propensities $q(A) \in \Delta^{F-1}$ (see Section 6.6 for the definition of $z(A)$).

Precomputation: rule activity and recommendations. For each menu A_t and each rule $f \in \mathcal{F}$, we compute once-and-for-all the indicators $A_f(A_t)$ and $L_f(A_t)$ defined in (1)–(2). These

are deterministic functions of (A_t, f) . Precomputing them is important: it makes training fast and ensures that the gate is the only learned component.

Gate estimation. On a given training split, we estimate the gate parameters θ by minimizing the training MSE between the predicted choice probability $g_{\text{RG}}(A; \theta)$ and the target $\hat{p}(A)$, where

$$g_{\text{RG}}(A; \theta) = \frac{\sum_{f \in \mathcal{F}} q_f(A; \theta) L_f(A)}{\max\{\sum_{f \in \mathcal{F}} q_f(A; \theta) A_f(A), m_{\min}\}}.$$

The gate weights $q_f(A; \theta)$ are given by the softmax specification (4). We optimize the smooth objective using Adam with gradient clipping. This training step is conceptually simple: it is standard least-squares fitting, except that predictions are constructed as a weighted average of deterministic rule recommendations, conditional on rule activity.

Interpretation. The estimated gate $q(A; \theta)$ can be read as a context-dependent mixture over simple procedures: for menus where a rule is inactive, it is effectively excluded by the activity filter; among active rules, the gate distributes probability mass so that the resulting mixture best matches observed choice frequencies.

6.6 Gate features

The gate’s role is to modulate rule responsibilities using observable features of the menu. A natural question is which features to use. We adopt as the baseline specification a 12-dimensional vector of economically motivated summary statistics $z(A) \in \mathbb{R}^{12}$. Six are *pairwise gaps* between the two lotteries: the expected-value gap $\text{EV}(L^1) - \text{EV}(L^2)$, the best-case outcome gap $\max(L^1) - \max(L^2)$, the worst-case outcome gap $\min(L^1) - \min(L^2)$, the variance gap $\text{Var}(L^1) - \text{Var}(L^2)$, the modal-outcome gap $\text{Mode}(L^1) - \text{Mode}(L^2)$, and the skewness gap $\text{Skew}(L^1) - \text{Skew}(L^2)$. These gaps are designed to capture the contrasts that the rules in the library operate on: the min/max gaps relate to MMN/MMX, the mode gap relates to MAP, and the EV and variance gaps relate to risk-return tradeoffs. The remaining six are *level variables*: the expected values $\text{EV}(L^1)$ and $\text{EV}(L^2)$, the standard deviations $\text{SD}(L^1)$ and $\text{SD}(L^2)$, the largest absolute outcome across both lotteries $\max_{i \in \{1,2\}} \max |\text{Supp}(L^i)|$, and the support-size gap $|\text{Supp}(L^1)| - |\text{Supp}(L^2)|$. The level variables allow the gate to condition rule propensities on the scale and complexity of the menu environment. By construction, $d_z = 12$ is much smaller than the $4M = 40$ dimensions of the raw encoding, but it captures the economically relevant variation: each feature has a direct verbal interpretation as a lottery comparison or a menu characteristic.

Why coarsen the gate input. Using a coarsened feature vector $z(A)$ rather than the raw menu encoding $\psi(A)$ is conceptually appropriate for the gate’s role. The gate is meant to capture systematic variation in rule usage with broad menu characteristics - scale, risk, tails, complexity - not to index menus individually. Coarsening yields repeated support points: many distinct menus share the same (or nearby) feature value $z(A)$, which is needed for the global identification conditions (G1)-(G2) to be empirically meaningful. With the raw 40-dimensional encoding, the mapping $A \mapsto \psi(A)$ is essentially injective, so the sufficient within-feature variation required by (G1) cannot literally occur. Finally, $z(A)$ is interpretable and portable across datasets, and in our application it matches or improves predictive accuracy relative to the raw encoding (Appendix N).

The gate uses the softmax architecture of Equation (4) with $z(A)$ in place of $\psi(A)$, giving $(|\mathcal{F}| - 1) \times (1 + d_z)$ free parameters. All neural benchmark models (Neural EU/PT/CPT, Value-Based, Context-Dependent, MOT) continue to use the raw encoding $\psi(A)$ as input, since they do not have a gate structure and the identification conditions do not apply to their parameterizations.

7 Results

This section reports out-of-sample predictive performance of the learned random rule model relative to the benchmark suite of Peterson et al. (2021), followed by completeness and restrictiveness diagnostics and a portability evaluation.

7.1 Predictive performance

Table 1 reports mean test Mean Square Error (MSE) across 50 random train/test splits, with learning-rate selection as described in Section 6. The main finding is that the rule-gating predictor substantially outperforms the standard structured models (Neural EU/PT/CPT and Value-Based), while remaining competitive with the two strongest flexible benchmarks.

Concretely, rule-gating improves on the Value-Based model and on all Neural EU/PT/CPT baselines by a substantial margin. These gains indicate that a small repertoire of transparent “lines of conduct,” combined with a flexible gate that learns when each procedure applies, captures substantial regularity in the data that is missed by standard preference-based architectures. Rule-gating also outperforms the flexible Context-Dependent model. Only the Mixture of Theories (MOT) achieves a lower MSE, consistent with the fact that this model allows richer menu interactions than any fixed rule library.⁶

Figure 1a visualizes the same comparison with uncertainty bands across splits. Performance differences are stable across splits, and the ranking is preserved across learning-rate choices in our grid. Figure 1b reports a complementary “learning-curve” diagnostic, plotting test-set MSE as a function of the fraction of training data used. Two patterns emerge. First, the learning curve of rule-gating tracks that of the fully context-dependent network and outperforms it across training fractions, suggesting that an interpretable rule-based structure extracts at least as much predictive content as a fully flexible context-dependent architecture. Second, rule-gating exhibits a clear and persistent improvement over the value-based network throughout the range of training fractions, consistent with the view that allowing menu-dependent selection among a small repertoire of procedures adds predictive content beyond a single flexible value representation. Finally, MOT continues to perform best across the curve, reflecting the additional flexibility afforded by a richer mixture-of-experts structure.

The trial-weighted metric MSE_w (Table 1) confirms that the ranking of models is stable when predictions are weighted by the precision of the observed choice frequencies: all pairwise orderings are preserved, and the magnitude of the gaps changes only marginally. Appendix Table A.2 reports split-level comparisons: for each pair of models, per-split metric differences are computed at the best learning rate, and we report the mean and standard error across 50 splits. Appendix

⁶A caveat on feature sets: the rule-gating model’s effective inputs include both the 12-dimensional gate features $z(A)$ and the 24-dimensional rule activity and recommendation indicators, which are nonlinear functions of the lottery primitives. The neural benchmarks operate on the raw 40-dimensional encoding $\psi(A)$ with small, generic architectures. The comparison therefore does not hold features fixed; the sklearn comparison in the appendix provides the closest feature-controlled evaluation.

Table A.3 reports split-variability intervals constructed from fold-to-fold variability across the 50 random splits. These intervals summarize how performance varies with the resampling of train/test partitions.

Interpretability–accuracy tradeoff. A gradient-boosted tree ensemble (GBT) trained on raw lottery summary statistics achieves MSE 0.0100 (Appendix Table A.9), meaningfully below both rule-gating (0.0128) and MOT (0.0114). The interpretability cost of the RRM is therefore non-trivial. We view this as a worthwhile tradeoff because the RRM’s interpretability is *structural*, not post-hoc: for each menu, it decomposes the prediction into contributions from named behavioral procedures with economically interpretable weights. Post-hoc explainability tools identify which *features* matter but cannot decompose predictions into named *procedures*. This structural decomposition, together with the identification guarantees of Section 3, is what permits the mechanism-level analysis of Section 8.

Table 1: Out-of-sample predictive performance (50 random splits). Learning rates are selected by inner-fold validation MSE (Pass A); test MSE and MSE_w are evaluated at the selected learning rate on the held-out test set (Pass B). MSE_w denotes the trial-weighted MSE defined in (20).

Model	Mean MSE	SD	Mean MSE_w	Best LR
MOT	0.01139	0.00056	n.a.	0.001
Rule-gating	0.01282	0.00059	0.01269	0.010
Context-dependent	0.01344	0.00081	0.01330	0.010
Value-based	0.01921	0.00081	0.01904	0.010
Neural PT	0.02064	0.00085	0.02050	0.010
Neural CPT	0.02145	0.00093	0.02134	0.010
Neural EU	0.02215	0.00085	0.02205	0.010

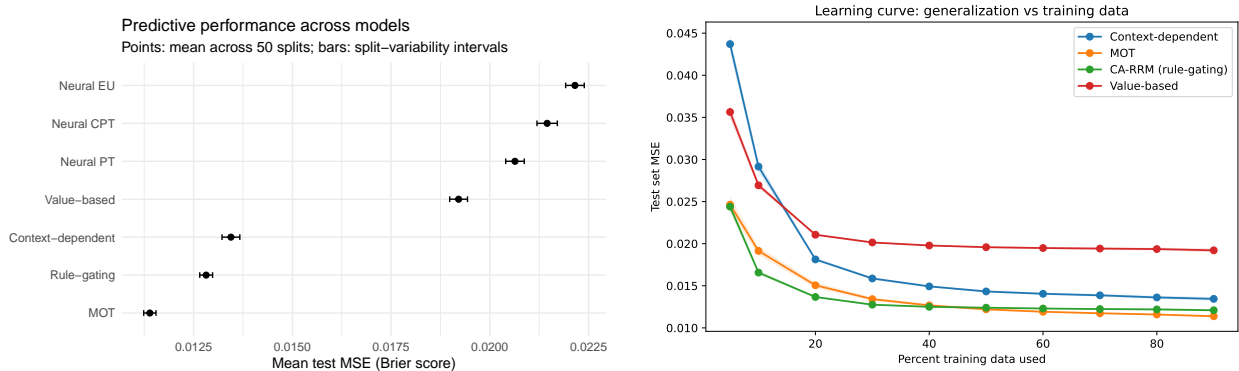
Note: †MOT learning rate is selected by test MSE following the published protocol of Peterson et al. (2021) (see Section 6.4); the HURD framework does not produce per-menu predictions, so MSE_w is unavailable for MOT in cross-validation. Rule-gating here uses the full 12-rule library. Approximate parameter counts: Neural EU/PT/CPT \approx 60–120; Value-based \approx 200; Context-dep. \approx 200; Rule-gating 143; MOT: see Peterson et al. (2021).

7.2 Completeness and Restrictiveness

Table 1 reports absolute out-of-sample predictive performance across models. In this section we add two complementary diagnostics that help interpret these performance differences. First, we measure *completeness*: how much of the predictive gains delivered by a highly flexible benchmark can be recovered by a more structured (and potentially interpretable) model. Second, we measure *restrictiveness*: how strongly a model class constrains the set of menu-to-choice mappings it can fit. Jointly, these measures help distinguish performance gains that reflect substantive structure from gains that could arise from sheer flexibility.

Machine Learning (ML) Completeness Score

While Table 1 reports absolute predictive performance, it is also useful to quantify how much of the predictive gains delivered by the strongest flexible architecture can be recovered by an



(a) Mean test MSE across 50 random splits (split-variability band). (b) Learning curve: test MSE vs. training fraction (split-variability band).

Figure 1: Predictive performance. Panel (a) compares out-of-sample MSE across models. Panel (b) reports the learning curve, plotting test-set MSE as a function of the percent training data used.

interpretable model. To this end, we compute a ML completeness measure inspired by recent work on the completeness of economic models (e.g., Peysakhovich and Naecker (2017), Fudenberg and Puri (2022), Fudenberg and Liang (2020), and Fudenberg et al. (2022)). We take Neural EU as the baseline model, since it is the most basic model in our benchmark class, and we take the Mixture of Theories (MOT) as the flexible benchmark. For any model class g , we define its ML completeness score by

$$\text{Comp}(g) := \frac{\text{MSE}(g_{\text{EU}}) - \text{MSE}(g)}{\text{MSE}(g_{\text{EU}}) - \text{MSE}(g_{\text{MOT}})}. \quad (22)$$

This statistic measures the fraction of the baseline-to-MOT improvement in out-of-sample MSE captured by g . By construction, $\text{Comp}(g_{\text{EU}}) = 0$ and $\text{Comp}(g_{\text{MOT}}) = 1$. Values in $(0, 1)$ indicate partial recovery of MOT’s predictive gains, values above 1 indicate that a model outperforms MOT, and negative values indicate performance below the baseline. The score depends on the choice of endpoints: using a different baseline (e.g., Neural PT instead of Neural EU) or a different flexible benchmark would rescale the numbers, though ordinal rankings across models would be preserved.

Figure 2a visualizes the ML completeness scores implied by Table 1. The rule-gating model closes a substantial fraction of the baseline-to-MOT performance gap ($\approx 87\%$), markedly exceeding the Value-based architecture ($\approx 27\%$). This normalization emphasizes that the predictive gains delivered by rule-gating are not marginal improvements over the expected utility benchmark, but a sizable step toward the performance of the strongest flexible models.

Restrictiveness

A complementary question is *restrictiveness*: how tightly a model class constrains the set of menu-to-choice mappings it can fit (Selten, 1991; Fudenberg et al., 2026). Following Fudenberg et al. (2026), we operationalize this by asking how well a model can fit structureless targets. Let π be a random permutation of the training menus \mathcal{T} and define permuted targets $\hat{p}^\pi(A) := \hat{p}(\pi(A))$. For each model class $g(\cdot; \theta)$, we re-estimate parameters on the permuted targets using the same architecture, the same learning rate selected from the main analysis (Table 1), and the same training horizon—but *without* re-running the inner learning-rate search. We define *permutation-fit*

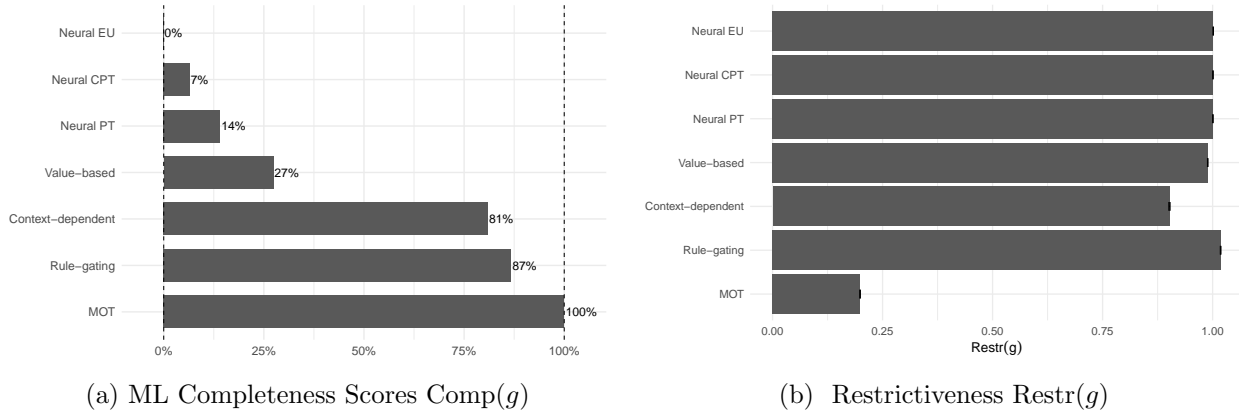


Figure 2: Completeness and Restrictiveness.

restrictiveness as the ratio of the model’s in-sample MSE on permuted targets to the error of the best constant predictor for those targets:

$$\text{Restr}(g) := \mathbb{E}_{\mathcal{T}, \pi} \left[\frac{\text{MSE}_{\text{train}}^{\pi}(g)}{\text{MSE}_{\text{train}}^{\pi}(\text{const})} \right], \quad (23)$$

where the expectation averages over the same $K = 50$ train/test splits and $P = 10$ independent permutations per split. Values near 1 indicate that the model cannot fit permuted targets better than a constant predictor (highly restrictive); values well below 1 indicate that it can absorb structureless patterns (weakly restrictive). In finite samples $\text{Restr}(g)$ can slightly exceed 1 when optimization or regularization prevents the model from matching the constant baseline on permuted data.

Model-wise restrictiveness. Figure 2b reports $\text{Restr}(g)$ for each model. MOT stands out as markedly less restrictive ($\text{Restr} \approx 0.2$), and the context-dependent architecture is moderately flexible ($\text{Restr} \approx 0.9$). All other models—including rule-gating and the neural utility benchmarks—have restrictiveness very close to 1, implying that they cannot improve meaningfully over a constant predictor on permuted targets.

Figure 3 plots each model in the (completeness, restrictiveness) plane. The neural utility benchmarks cluster at high restrictiveness but low completeness; MOT achieves maximal completeness with low restrictiveness. Rule-gating and context-dependent occupy the upper-right region: the context-dependent model is more complete but less restrictive, whereas rule-gating is more restrictive but somewhat less complete. These results suggest that rule-gating delivers a large share of the predictive gains of flexible benchmarks while retaining strong discipline against fitting arbitrary mappings.

7.3 Portability

Finally, a central motivation for interpretable decision procedures is that they are intended to capture stable regularities of behavior, not merely to interpolate within a single dataset. A natural final check is therefore *portability*: does a predictor trained on one large-scale choice environment

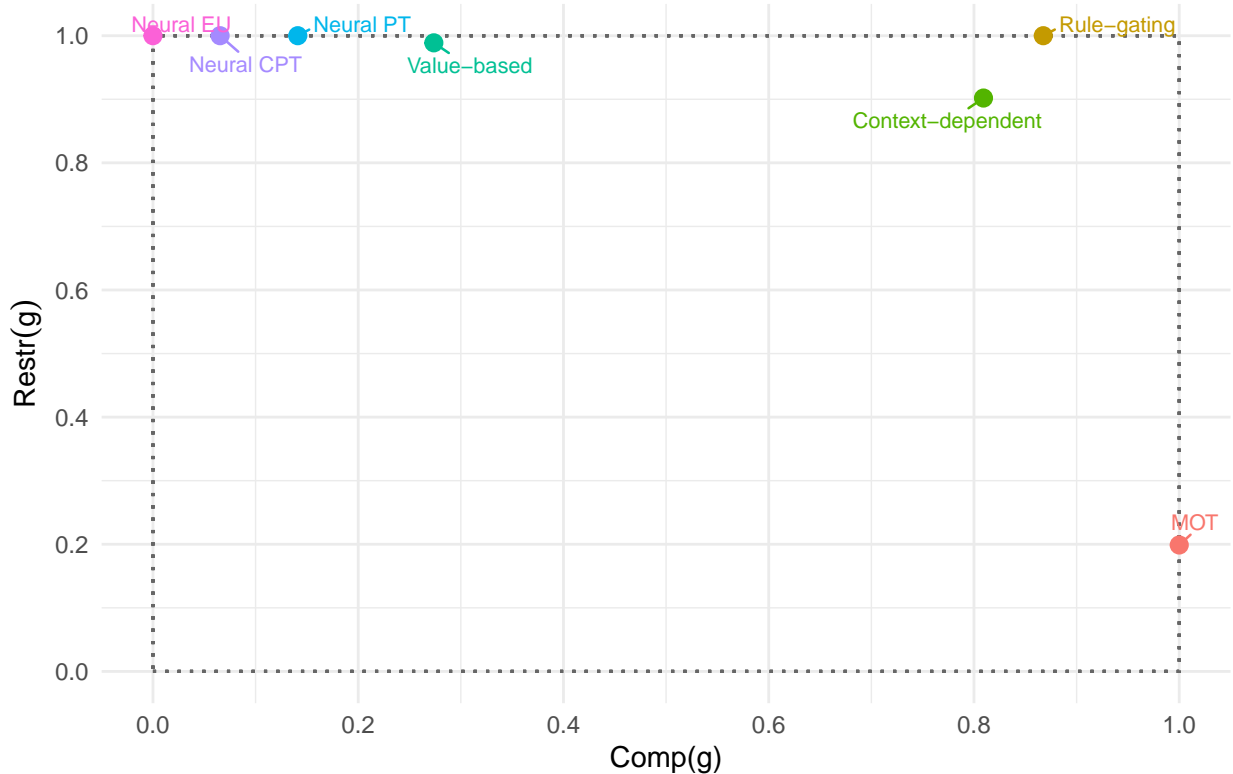


Figure 3: Completeness–restrictiveness plot. The horizontal axis is ML completeness (Equation (22)); the vertical axis is permutation-fit restrictiveness (Equation (23)).

retain predictive content when exported - without re-tuning - to an independent dataset with different subjects and a different menu sample?

To assess portability, we evaluate the models trained on `choices13k` (Peterson et al., 2021) on an independent dataset of binary lottery choices, the publicly available CPC18 competition dataset (Erev et al., 2017; Plonsky et al., 2017).⁷ We restrict attention to the risk problems and exclude ambiguity tasks. The resulting sample comprises $N = 686$ subjects recruited across multiple locations in Israel. Each subject faces 20 to 28 distinct binary lottery choice problems, and each problem is repeated for 25 trials, yielding 500 to 700 decisions per subject. The design includes both no-feedback and feedback regimes.

Because `choices13k` reports aggregate choice frequencies by menu, we aggregate CPC18 to the menu level by computing, for each unique binary menu A , the empirical left-choice frequency $\hat{p}_{\text{CPC}}(A)$ across all available repetitions (and subjects). This produces a dataset of $|\mathcal{A}^{\text{CPC}}| = 180$ distinct menus and 354,400 total trials (the product of the 686 subjects and their individual problem counts, each repeated 25 times).⁸ Although CPC18 is much smaller than `choices13k`, it provides a stringent out-of-domain test of whether a learned mapping from menu features to choice probabilities generalizes beyond the environment on which it was trained.

⁷The data can be downloaded at <https://cpc-18.com/data/>.

⁸In addition to the unweighted menu-level aggregation, we also consider a trial-weighted evaluation that weights each menu by its number of observations.

Portability design. For each model class, we estimate parameters on `choices13k` exactly as in Section 6.4, using the model-specific learning rate selected in Table 1. We then freeze these parameters and apply the fitted predictor to the CPC18 menus. Let \mathcal{A}^{13k} denote the filtered `choices13k` analysis set and let \mathcal{A}^{CPC} denote the set of binary menus in CPC18 after applying the same basic preprocessing (e.g., removing masked probabilities when relevant). Using the parameters learned on `choices13k`, each model produces a portability prediction $g_{\rightarrow}(A) \in [0, 1]$ for each $A \in \mathcal{A}^{\text{CPC}}$. We evaluate portability using the same mean-squared error metric:

$$\text{MSE}_{\text{CPC}}(g_{\rightarrow}) := \frac{1}{|\mathcal{A}^{\text{CPC}}|} \sum_{A \in \mathcal{A}^{\text{CPC}}} \left(g_{\rightarrow}(A) - \hat{p}_{\text{CPC}}(A) \right)^2. \quad (24)$$

All models use the same menu encoding $\psi(A)$ as in (21). The outcome rescaling factor (maximum absolute payoff) is computed from the `choices13k` training sample and applied identically to CPC18 outcomes, so that the feature space is consistent across datasets.⁹ No hyperparameters are tuned on CPC18: MSE_{CPC} is a pure out-of-domain test. Models are exported without re-tuning.

Trial-level evaluation. Because CPC18 records individual-level trial data, we also evaluate portability at the trial level using the Brier score and Bernoulli log-loss, which assess each menu-level prediction against realized binary choices. Trial-level evaluation is the primary portability metric; menu-level MSE is retained for comparability (Appendix Table A.7).

Portability results. Table 2 reports portability metrics for the full set of models. Two patterns stand out. First, models that perform well in-sample on `choices13k` are not necessarily portable: notably, MOT—the most flexible benchmark and the best performer in Table 1—performs poorly under transfer, suggesting that a substantial share of its predictive advantage is dataset-specific and does not export cleanly to a different menu distribution and subject pool. Second, the rule-gating model retains strong predictive content under transfer: it achieves CPC18 MSE 0.0170, essentially tied with the context-dependent model (0.0172) and far ahead of the structured neural benchmarks (≈ 0.032). The margin between rule-gating and the context-dependent model is small relative to the CPC18 sample size (180 menus) and should not be over-interpreted; the salient finding is that both models transfer well while MOT does not. Rule-gating therefore offers strong portability *with* an interpretable behavioral decomposition, whereas the context-dependent model — despite similar transfer accuracy — is a black-box predictor.

8 Mechanisms

We now examine the behavioral mechanisms underlying rule-gating’s predictive performance. The responsibility weights w_f and context-dependent patterns reported below are *population-level* objects: they describe how the fitted mixture varies across menus in a dataset aggregating choices across many individuals. This is consistent with within-individual variation in rule use, between-individual heterogeneity, and noise. Without individual-level panel data, these components cannot be separated; mechanism-level statements should be read as describing population-level reallocation.

⁹Because both datasets use a common monetary unit (points/tokens), the rescaling factor simply puts all outcomes on a common numerical scale. No currency conversion is required.

Table 2: Portability to CPC18: models trained on `choices13k` and evaluated on CPC18 without re-tuning. Trial-level Brier score and log-loss use individual choice observations ($n = 354,400$); menu-level MSE aggregates to the menu level ($n = 180$).

Model	Brier _{trial}	LogLoss _{trial}	MSE _{menu}
Rule-gating	0.1971	0.5747	0.0170
Context-dependent	0.1977	0.5760	0.0172
Neural CPT	0.2111	0.6112	0.0320
Neural EU	0.2114	0.6122	0.0320
Value-based	0.2120	0.6142	0.0321
Neural PT	0.2121	0.6136	0.0326
MOT	0.2691	0.7480	0.0926

Note: Brier_{trial} and LogLoss_{trial} evaluate each model’s predicted menu-level probability against individual binary choices. All models are trained once on the full Choices13k sample and evaluated on CPC18 without re-tuning.

8.1 Responsibility weights w_f

Figure 4 reports the fitted rule-responsibility weights w_f for the full 12-rule model, computed as average *conditional-on-activity* responsibilities:

$$w_f = \mathbb{E}_A \left[\tilde{q}_f(A; \hat{\theta}) \right], \quad \tilde{q}_f(A; \theta) = \frac{q_f(A; \theta) A_f(A)}{\sum_{g \in \mathcal{F}} q_g(A; \theta) A_g(A)}.$$

Recall that w_f measures the average share of decision mass attributed to rule f among *decisive rules*. We refer to w_f as the *responsibility* (or attribution) weight of rule f , since it reflects the fraction of the predicted choice probability that can be attributed to that rule in the fitted mixture, rather than a direct observation of which rule a decision-maker “uses.”

Two patterns stand out. First, the attention rules A1 and A2 absorb the two largest shares of effective responsibility ($w_{A1} \approx 0.193$ and $w_{A2} \approx 0.146$), with a combined attention weight of about 34%. This is expected: the attention rules are decisive on essentially all menus and serve as a catch-all channel. Among the other rules, MMN (security, 15.7%), MMX (aspiration, 11.4%), SAL (most salient comparison, 10.7%), and MAP (modal payoff, 8.5%) carry the largest responsibility weights. Second, because multiple rules are typically active on the same menu (on average, about 5.8 rules are both active and consistent with the majority choice direction), these responsibility weights reflect the outcome of competition among substitutable procedures rather than mechanical assignment to the only available rule.

It is useful to separate the library into two conceptual channels. The *structured rules* (MMN, MMA, MMX, MAP, SAL, SAL2, REG, REGMED, DIS, DISMED) encode distinct behavioral mechanisms that generate non-trivial, menu-dependent recommendations. The *attention channel* (A1 and A2) captures inattention, hasty responding, or trembling: A1 always recommends left and A2 always recommends right, regardless of lottery content. These attention rules absorb about one-third of effective responsibility, reflecting the prevalence of default-like behavior in the online (MTurk) environment. Because the marginal left-choice frequency is $\bar{p} \approx 0.510$ (essentially one-half), this weight cannot be explained by aggregate position bias; rather, the gate allocates attention weight in a menu-dependent way. Part of this weight may, however, reflect absorption of residual prediction error by always-active rules rather than a cleanly identified behavioral channel.

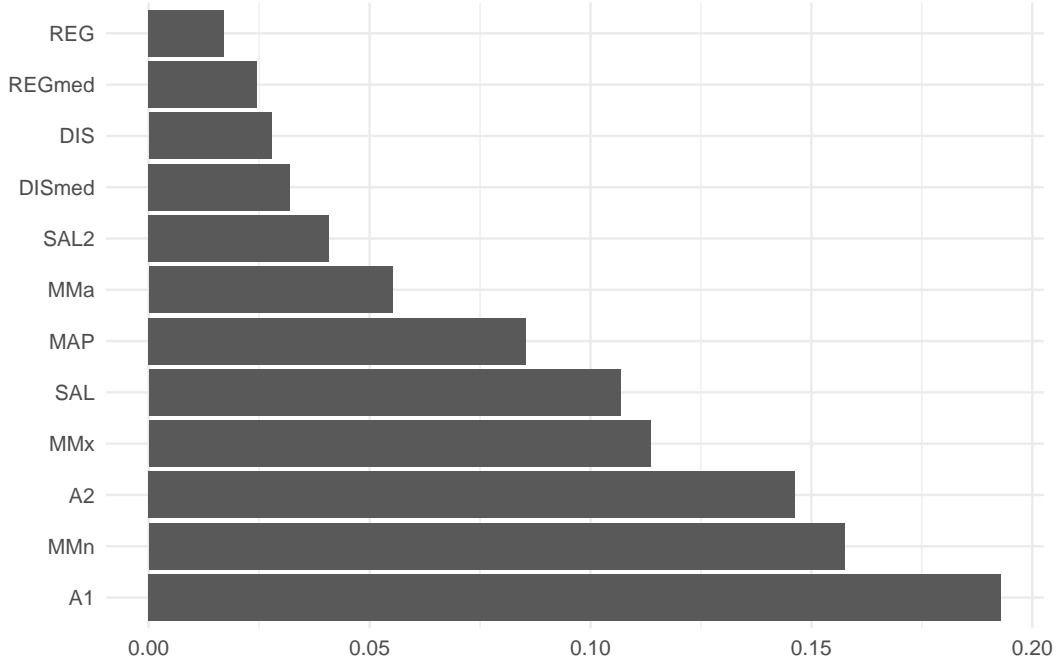


Figure 4: Rule responsibility weights w_f for the full 12-rule library. Each w_f is the average share of predicted choice probability attributed to rule f among decisive rules.

Our interpretability claims concern the *structured rules conditional on the inattention channel*. Section 9.4 confirms that mechanism patterns persist when the attention channel is removed entirely.

To summarize how concentrated effective responsibility is, we report

$$\text{HHI}(F) = \sum_{f \in \mathcal{F}} w_f^2, \quad N_{\text{eff}}(F) = \frac{1}{\text{HHI}(F)}.$$

In our estimates, $\text{HHI}(F) \approx 0.122$ and $N_{\text{eff}}(F) \approx 8.2$ (see Figure 4). For comparison, uniform weights across all 12 rules would give $\text{HHI} = 1/12 \approx 0.083$ and $N_{\text{eff}} = 12$. The observed concentration is therefore moderately above the uniform benchmark — driven primarily by the attention channel — but far from the winner-take-all extreme ($\text{HHI} = 1$).

8.2 Rule concentration

We next quantify which procedures are necessary for predictive fit. Figure 5a reports the ablation index $\phi(f)$, the relative change in test MSE when rule f is removed from the full library and the gate is retrained on the reduced set. We ablate each of the 10 behavioral rules (excluding attention rules A1/A2, which serve a structural role ensuring decisiveness at every menu). A small subset of rules drives most of the predictive gains: removing SAL2 or SAL produces the largest deterioration, followed by MMX, MMN, and REGMED. Notably, SAL2 has a relatively high ablation impact despite carrying a lower average responsibility weight than MMN or SAL; this illustrates the distinction between w_f (average usage) and $\phi(f)$ (marginal predictive contribution), and suggests that the second-most-salient comparison provides incremental content not replicated

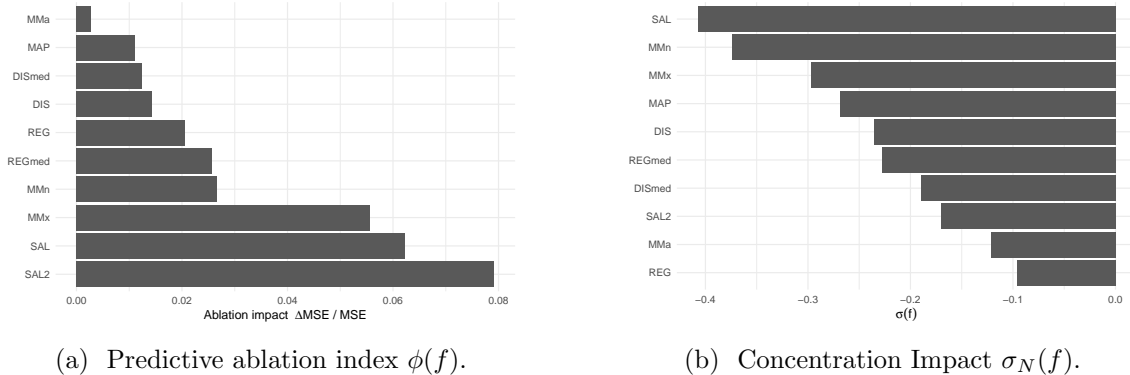


Figure 5: Rule diagnostics: ablation of each behavioral rule from the full 12-rule library. Error bars show split-variability intervals ($\pm 1.96 \times \text{SE}$) from fold-to-fold variability across 50 CV splits.

by other rules. By contrast, removing MAP, MMA, REG, or DIS/DISMED has little effect on MSE, suggesting that these rules are largely redundant given the rest of the library (or apply primarily in regions of menu space that contribute little to aggregate loss).

Ablations identify rules that matter for accuracy, but they do not indicate whether a rule acts as a *unifier* (concentrating effective responsibility on a small repertoire) or as a *substitute* that diversifies the fitted mixture. To capture this, in Figure 5b, we report the relative change in the effective number of rules $\sigma_N(f)$. We find that $\sigma_N(f)$ is negative for all non-attention rules: when any single rule is removed, the refitted gate reallocates responsibility more sharply onto a smaller set of remaining procedures. The magnitude is largest for the same procedures that have large ablation impacts, indicating that these rules both attract mass and shape the overall mixture structure.

Overall, predictive accuracy is driven by a small set of procedures—salience-based comparisons and extreme-outcome comparisons—as evidenced by their large $\phi(f)$, while the responsibility weights w_f additionally highlight modal-outcome comparisons (MAP) as receiving substantial mass despite a modest ablation impact. The remaining rules do not simply “sit idle”: their negative $\sigma_N(f)$ values show that they act as substitutes that diversify the fitted mixture. Appendix Table A.4 reports split-variability intervals for $\phi(f)$, confirming that the main rankings are stable. Such a decomposition is not available in the more flexible predictors that outperform rule-gating, and it provides a transparent characterization of which bounded-rationality mechanisms are empirically relevant in a large dataset of choice under risk.

8.3 Drivers of rule selection

Complexity

A central motivation for rule-gating is that a fixed decision rule is too coarse to account for behavior across the wide range of menus in `choices13k`. The substantive hypothesis is therefore not merely that people are noisy, but that they adaptively select different procedures across menus. To connect this hypothesis to the emerging literature on complexity and procedure choice, we rely on an objective notion of menu complexity that is defined directly from the two lotteries in the menu and is available ex ante. This notion is designed to capture when a choice problem requires trading off state-by-state advantages and disadvantages across the two options—precisely the situations where

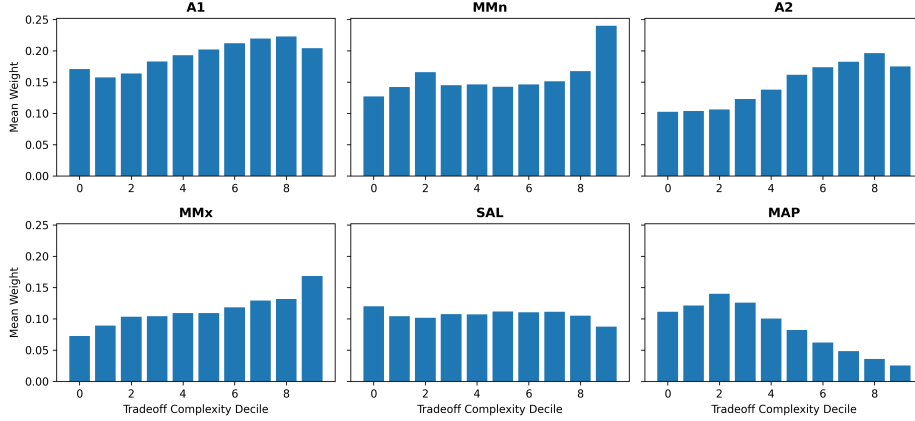


Figure 6: Mean effective responsibility weights across deciles of tradeoff complexity $TC(A)$ for the highest-weight rules.

different heuristics can plausibly disagree and where a gate has something non-trivial to learn.

In binary lottery choice, a particularly natural notion is *tradeoff complexity*. Formally, for a menu $A = \{L^1, L^2\}$, let F_1 and F_2 denote the cumulative distribution functions of the two objective lotteries (after placing their supports on a common ordered grid). Define the CDF distance

$$\Delta_{\text{CDF}}(A) := \int_{\mathbb{R}} |F_1(x) - F_2(x)| dx,$$

and the associated *excess dissimilarity*

$$d(A) := \Delta_{\text{CDF}}(A) - |EV(L^1) - EV(L^2)|.$$

The subtraction removes the mechanical effect of a pure value gap and isolates the extent to which the two lotteries “cross” in payoff space, i.e., the extent to which the comparison requires genuine tradeoffs rather than a near-unanimous ordering. In the empirical analysis we work with the log-transformation $TC(A) := \log(1 + d(A))$ and plot mean effective responsibility weights across complexity deciles.

Figure 6 shows clear and interpretable shifts in rule selection along tradeoff complexity. As $TC(A)$ increases, the two attention rules (A1/A2) display a pronounced increase in mean effective weight, consistent with the view that more complex menus are associated with a greater reliance on coarse inattention in the learned CA-RRM. Among the structured procedures, MMX (aspiration/extreme-max comparison) rises with complexity, whereas MAP (modal payoff comparison) declines; SAL and MMN are comparatively stable across deciles. Overall, increasing tradeoff complexity appears to tilt the fitted mixture away from modal-outcome comparisons and toward more extreme-outcome and attention-based procedures.

The same exercise for the full library (Appendix Figure A.3) reveals additional structure among secondary rules: in particular, regret- and disappointment-type procedures (REG/REGMED and DIS/DISMED) exhibit a decline in weight as complexity increases, suggesting that these more evaluative comparative procedures play a smaller role in high-tradeoff menus relative to simpler screening and extreme-outcome mechanisms.

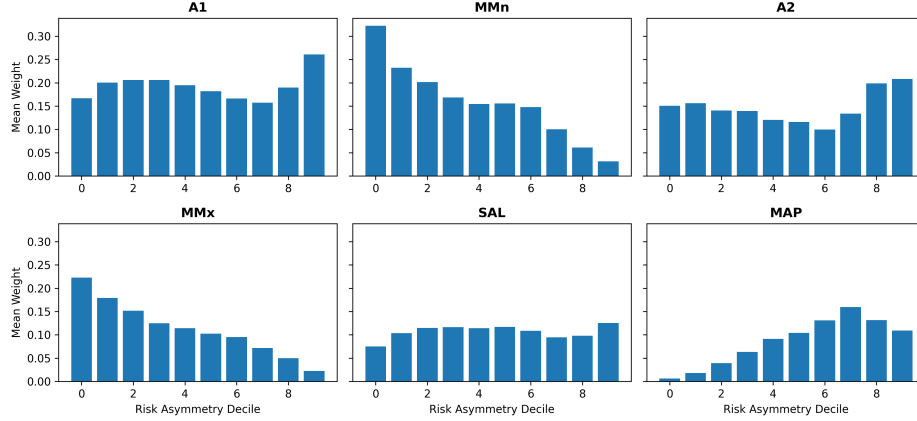


Figure 7: Mean effective responsibility weights across deciles of risk asymmetry $\text{RiskAsym}(A)$ for the highest-weight rules.

Risk

A second natural driver is the risk profile of the menu. Different procedures emphasize different aspects of risk, such as dispersion, downside exposure, and sensitivity to rare events. As a first-pass risk descriptor available directly from the menu, we consider the signed asymmetry in dispersion across the two lotteries,

$$\text{RiskAsym}(A) := \sigma(L^1) - \sigma(L^2),$$

where $\sigma(L)$ denotes the standard deviation of lottery L . This is a directional measure: positive values indicate that L^1 is more dispersed, and negative values indicate that L^2 is. Figure 7 plots mean responsibility weights across deciles of this signed difference, so that the x -axis runs from menus where L^2 is riskier (left) to menus where L^1 is riskier (right). We use the absolute value $|\text{RiskAsym}(A)|$ when referring to the magnitude of dispersion asymmetry without regard to direction.

Figure 7 provides a complementary view based on dispersion asymmetry. Along deciles of $\text{RiskAsym}(A)$, the fitted mixture shifts away from extreme-outcome comparisons: both MMN (security) and MMX (aspiration) show a clear decrease in mean weight as risk asymmetry increases. By contrast, the attention rules and SAL remain relatively flat, while MAP displays an increasing pattern. Thus, in menus where dispersion is more asymmetric across the two options, the gate reallocates mass away from max/min-type screening and toward modal-outcome comparisons, with attention and salience mechanisms playing a more stable background role. More secondary rules show less systematic movements with risk (Appendix Figure A.4).

These diagnostics show that rule selection varies systematically with salient menu primitives: along complexity, the mixture tilts toward inattention and extreme-outcome screening and away from modal-outcome comparisons; along dispersion asymmetry, the shifts reverse on key dimensions. Menu-dependent selection across a small repertoire of procedures is economically meaningful.

Table 3: Rule-level coverage and side-variation (D2). For each rule f , N_{act} is the number of menus where f is decisive, $\Pr(L \mid \text{act})$ and $\Pr(R \mid \text{act})$ are the conditional left/right recommendation frequencies. Rules that take both sides contribute sign-varying rows to $H^{(k)}$, supporting condition (G1).

Rule	N_{act}	$\Pr(\text{act})$	$\Pr(L \mid \text{act})$	$\Pr(R \mid \text{act})$	Switches
MMN	9,584	0.975	0.294	0.706	✓
MMA	9,668	0.983	0.580	0.420	✓
MMX	9,688	0.985	0.739	0.261	✓
MAP	9,512	0.968	0.410	0.590	✓
SAL	9,831	1.000	0.485	0.515	✓
SAL2	4,057	0.413	0.509	0.491	✓
REG	2,951	0.300	0.544	0.456	✓
REGMED	8,661	0.881	0.446	0.554	✓
DIS	4,773	0.486	0.322	0.678	✓
DISMED	4,773	0.486	0.336	0.664	✓
A1	9,682	0.985	1.000	0.000	
A2	9,831	1.000	0.000	1.000	

9 Robustness

The RRM framework makes several modeling choices that could, in principle, drive its empirical performance: the composition of the rule library, the FOSD-based activation criterion, the use of interpretable gate features, and the softmax gating architecture itself. This section subjects each of these choices to targeted robustness checks. We begin with the identification diagnostics and decomposition stability (Section 9.1), then document library coverage, before turning to directed tests: cross-fitted library selection, attention-rule removal, variation of the activity discipline, and three further checks (placebo test, feature-based baselines, raw-encoding gate) reported in the appendix.

9.1 Identification diagnostics

We evaluate diagnostics D1–D3 on the full Choices13k dataset.

D1. 9,823 of 9,831 menus (99.9%) are two-sided, confirming that the log-odds representation (9) is well-defined on virtually the entire sample.

D2. Table 3 reports per-rule coverage and side-variation. All ten non-attention rules switch sides, and all but one (REG, 30%) are decisive on at least 41% of menus, contributing sign-varying rows to the $H^{(k)}$ matrices that drive condition (G1). The attention rules (A1, A2) are each confined to a single side by construction.

D3. Table 4 reports the empirical support for conditions (G1) and (G2) of Theorem 1, evaluated on the baseline gate features $z(A) \in \mathbb{R}^{12}$. In the Choices13k data, the 12-dimensional features

Table 4: Global identification verification (D3). Conditions (G1) and (G2) of Theorem 1 are checked on the Choices13k data using k -means clustering on interpretable z -features ($d = 11$).

Condition	Value	Status
Effective feature dimension d_{eff}	11	
(G1) Cells with $\text{rank}(H^{(k)}) = \mathcal{F} - 1$	41 / 12 needed	✓
(G2) $\text{rank}([1, z])$	12 / 12 needed	✓
Globally identified		✓

are essentially unique across menus, so exact-equality cells are singletons. We supplement exact equality with k -means clustering on $z(A)$, grouping menus into 50 cells.¹⁰ Of these, 41 cells achieve $\text{rank}(H^{(k)}) = |\mathcal{F}| - 1$, well above the $d_{\text{eff}} + 1 = 12$ needed for (G1). Among the G1-passing cells, the augmented centroid matrix has full affine rank, satisfying (G2). Both conditions are supported. The rank conditions are structurally stable: because the relevant singular values are well above the SVD tolerance ($10^{-8} \times \sigma_1$), small perturbations in $\hat{r}(A)$ do not change the ranks.

Fold-level stability of the decomposition objects is reported in the appendix (Table A.5): the rule rankings by w_f and $\phi(f)$ are highly stable across independent training samples.

9.2 Library Coverage

It is useful to document that predictive fit is not driven by a knife-edge mapping from menus to a single decisive procedure. For each menu, let $N_{\text{cons}}(A)$ count the number of rules that are simultaneously active and consistent with the observed majority choice direction. Figure 8 reports the distribution across the 9,831 menus. Menus that pin down a unique decisive rule are rare ($\Pr[N_{\text{cons}}(A) = 1] \approx 0.16\%$), while overlap is substantial on average ($\mathbb{E}[N_{\text{cons}}(A)] \approx 5.8$). Moreover, the average number of active rules per menu is about 9.5 out of 12, so activity rarely collapses the library to a small subset. These diagnostics confirm that the gate is learning selection among genuinely competing procedures rather than exploiting mechanically unique recommendations.

9.3 Cross-fitted library restrictions

A potential concern with the rule library is that it was assembled *ex ante* by the researcher, and performance may depend on the particular collection of rules included. To address this, we implement a cross-fitted selection protocol that chooses rule subsets *only on training folds* and evaluates performance out of sample.

Top- k selection. For each CV fold, we fit the full rule-gating model (all 12 rules, including the attention rules) on the training set and compute the average effective responsibility w_f on the training data. We then rank all 12 rules by w_f and select the top- k (for $k \in \{3, 5, 7, 12\}$). For each k , we refit a restricted gate using only the selected rules on the same training set and evaluate on the held-out test set. The selection is “cross-fitted” in the sense that rule subsets are chosen

¹⁰The number of clusters (50) is chosen so that each cell contains at least $|\mathcal{F}| - 1$ menus while keeping within-cell feature variation modest. The result is qualitatively stable to alternative cluster counts (e.g., 30, 75, 100).

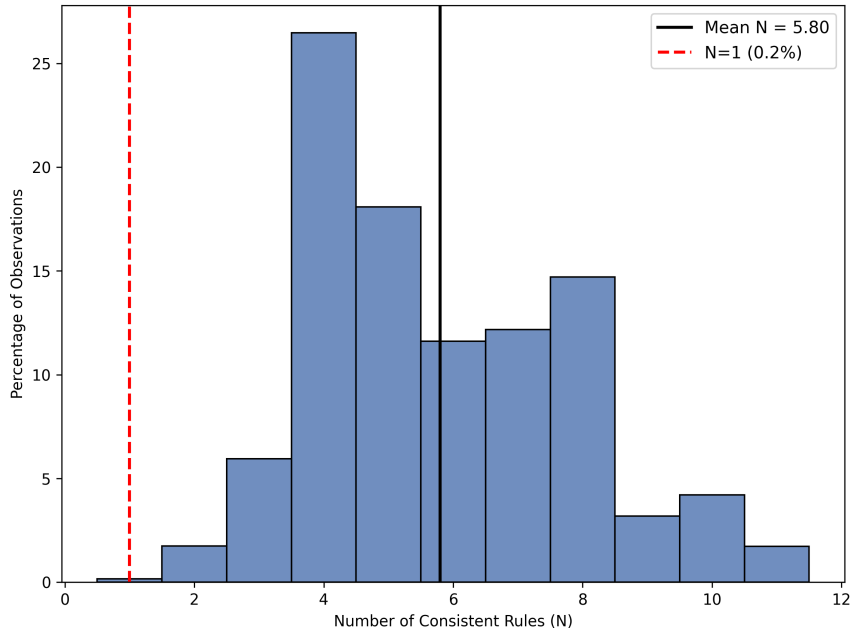


Figure 8: The histogram plots $N_{\text{cons}}(A)$.

using in-sample information only, and the restricted model’s performance is evaluated strictly out of sample.

Family selection. An alternative selection unit is the behavioral *family*: we group rules into five predefined families - extremum (MMN, MMA, MMX, MAP), salience (SAL, SAL2), regret (REG, REGMED), disappointment (DIS, DISMED), and attention (A1, A2) - and select the top- k_{fam} families (for $k_{\text{fam}} \in \{1, 2, 3, 4, 5\}$) by aggregate family responsibility on the training set. All rules within the selected families are included, and performance is again evaluated out of sample.

Table 5 reports results. The main finding is that performance retention is high even with substantial library reduction. Under top- k selection, restricting to $k = 7$ rules retains the bulk of the full-library predictive accuracy, with $k = 5$ still substantially outperforming a constant predictor, although at this level the model no longer clearly dominates all structured neural benchmarks. At $k = 3$, retention drops to about 25%, indicating that three rules are too few to span the behavioral variation in the data. Under family selection, two families suffice for strong performance, but restricting to a single family produces negative retention (MSE exceeding twice the full-library level), because no single family can substitute for the complementary mechanisms provided by the others. Selection is stable across folds: the rules that the full model weights most heavily are also the ones most frequently selected out of sample (see Appendix Table A.6 for fold-by-fold selection frequencies).

These results address the “handpicked library” concern in two ways. First, the identity of the selected rules is consistent with the main mechanism results in Section 8: the top-ranked rules in cross-fitted selection match the highest-responsibility rules in the full model. Second, the fact that small subsets retain strong performance confirms that the library’s predictive contribution is concentrated on a few core mechanisms rather than distributed thinly across many rules.

Table 5: Cross-fitted library restrictions: mean test MSE for top- k and top-family selections from the full 12-rule library. Subsets are chosen on training folds only; performance is evaluated out of sample.

Selection type	k	Mean MSE	SE	Retention (%)
Full (12 rules)	12	0.01248	0.00008	100.0
Top- k	7	0.01381	0.00010	89.3
Top- k	5	0.01548	0.00013	75.9
Top- k	3	0.02185	0.00020	24.9
Full (5 families)	5	0.01247	0.00007	100.0
Top-family	4	0.01268	0.00008	98.3
Top-family	3	0.01368	0.00010	90.3
Top-family	2	0.01596	0.00012	72.0
Top-family	1	0.02736	0.00024	-19.4

Note: Retention (%) = $100 \times [1 - (\text{MSE}^k - \text{MSE}^{\text{full}}) / \text{MSE}^{\text{full}}]$: 100% means no loss; values below 0% indicate MSE exceeds twice the full-library MSE. Selection is cross-fitted: rule subsets chosen on training data, evaluated on held-out test data.

9.4 Attention-rule removal

The attention rules absorb about one-third of effective responsibility ($w_{A1} \approx 0.193$, $w_{A2} \approx 0.146$), capturing a channel that is plausibly important in MTurk data where inattention and default-like behavior are prevalent. Table A.1 (Appendix) replicates the main cross-validation with the 10-rule model (excluding A1/A2). The 10-rule model achieves MSE 0.0201, outperforming Neural EU (0.0222), Neural CPT (0.0215), and Neural PT (0.0206), while remaining close to the value-based network (0.0192). This confirms that the attention channel carries substantial predictive content (MSE rises from 0.0128 to 0.0201), but the non-attention rules alone still surpass most structured benchmarks.

The qualitative context-dependent patterns also persist under the 10-rule specification: MMX rises with complexity while MAP declines, and along risk asymmetry, extreme-outcome comparisons decrease while MAP increases; see Appendix C, Figures A.1–A.2.

9.5 Varying the activity discipline

Our baseline activity discipline requires strict first-order stochastic dominance (FOSD) of the conduct-transformed lotteries. This threshold is sharp: a rule is active whenever the survival function of the recommended option weakly dominates and strictly exceeds the other at some point. We probe the sensitivity of the model to this discipline in two directions.

Strengthening the discipline ($\varepsilon > 0$). We require an ε -gap in the survival functions: specifically, $S^1(z) \geq S^2(z) + \varepsilon$ for all grid points z (beyond the common starting point) and $S^1(z) > S^2(z) + \varepsilon$ for at least one grid point.

For $\varepsilon \in \{0.01, 0.05, 0.10\}$, we rebuild the rule activity indicators and re-run the full 50-fold cross-validation protocol. Table 6 reports, for each ε , the mean number of active rules per menu,

the average overlap with the majority choice direction, and the out-of-sample MSE from the same CV protocol as Table 1.

As ε increases, the activity discipline becomes more stringent: fewer rules are active per menu, and the remaining active rules tend to be those with clearer dominance relationships. The key finding is that the overall structure of the activity pattern - in particular, the relative ranking of rules by mean activity - is robust to moderate increases in ε , although the absolute level of activity naturally decreases. On the predictive side, the MSE at $\varepsilon = 0.01$ remains close to the baseline, confirming that the model’s predictions do not hinge on marginal dominance relationships. At larger ε , fewer rules are available on each menu, and MSE increases, reflecting the loss of discriminatory power as the library becomes more conservative.

Removing the discipline ($\varepsilon < 0$). A complementary question is whether the FOSD-based activation *itself* carries predictive information, or whether the gate could achieve similar performance if all rules were declared active on every menu. To test this, we set $\varepsilon = -2$, which makes the dominance condition trivially satisfied: all 12 rules are active on every menu (mean active rules = 12). Recommendations for rules that have standard FOSD are preserved; rules for which neither direction dominates are assigned a default (right-option) recommendation, adding noise. All other aspects of the model - architecture, learning rate, training horizon - are held fixed.

Table 6 includes this specification. Without the activity discipline, MSE increases only modestly relative to the baseline (0.01294 vs. 0.01282), indicating that the gate is flexible enough to partially compensate by down-weighting rules that lack a clear dominance signal. Notably, the no-discipline specification ($\varepsilon = -2$) still outperforms all positive- ε variants, where genuinely informative rules are progressively removed. The pattern across the full range of ε values is therefore asymmetric: over-restricting the activity set (high ε) is more costly than under-restricting it (all rules active), because the former removes rules that carry genuine predictive content, while the latter only adds noise that the gate can learn to suppress.

This asymmetry clarifies the role of the FOSD-based activation: for *prediction*, the gate can largely learn on its own which rules to suppress, but for *interpretation*, the activation criterion ensures that responsibility weights are nonzero only on menus where the rule delivers a decisive ranking. The activation discipline is therefore best understood as an *interpretive* discipline rather than a predictive one.

9.6 Placebo rule library, feature-based baselines, and raw-encoding gate

Three additional robustness checks are reported in Appendix L–N. First, a *placebo test* scrambles each rule’s indicators across menus within complexity strata, preserving marginal activity and recommendation rates but destroying the menu-specific mapping. The placebo library produces substantially higher MSE than the real library (Appendix Table A.8), confirming that the rule indicators carry genuine, menu-specific predictive content.

Second, we benchmark against *feature-based baselines*: a fractional logit and a gradient-boosted tree ensemble (GBT), each trained on rule indicators, summary statistics, or both (Appendix Table A.9). On rule features alone, rule-gating substantially outperforms both baselines, showing that the activity-conditioned gate architecture extracts more from the rule library than standard classifiers (though the gate also conditions on $z(A)$, so the comparison is not purely architectural). GBT on raw summary statistics outperforms all structured models, but provides no behavioral decomposition.

Table 6: Activity discipline robustness: activity statistics and out-of-sample MSE under varied dominance thresholds. The baseline ($\varepsilon = 0$) corresponds to strict FSD; $\varepsilon > 0$ strengthens it; $\varepsilon < 0$ removes it (all rules active).

ε	Mean active rules	Mean overlap	Mean MSE	SD
-2.00	12.00	7.03	0.01294	0.00062
0.00	9.46	5.80	0.01282	0.00059
0.01	9.12	5.56	0.01307	0.00060
0.05	8.99	5.47	0.01364	0.00064
0.10	8.83	5.36	0.01413	0.00066

Note: For $\varepsilon \geq 0$, ε -FSD requires $S^1(z) \geq S^2(z) + \varepsilon$ for all z (with strict inequality somewhere). For $\varepsilon < 0$, all rules are declared active on every menu; recommendations follow standard FOSD where applicable. Mean active rules: average number of decisive rules per menu. Mean overlap: average number of active rules consistent with the majority choice direction. MSE is from the same 50-fold CV protocol as Table 1.

Third, a *raw-encoding gate* variant uses the full 40-dimensional menu representation $\psi(A)$ instead of $z(A)$ (Appendix Figure A.5). It achieves MSE 0.01464, about 14% worse than the baseline $z(A)$ specification (0.01282), confirming that the interpretable summary statistics capture decision-relevant variation without sacrificing accuracy. The global identification conditions (G1)–(G2) are not applicable to this parameterization.

Summary of robustness evidence

Taken together, these checks confirm that the gate is globally identified, that the decomposition is stable across training samples, and that the rule indicators carry genuine predictive content. Performance is not an artifact of the ex ante library choice, the attention channel, or the specific activity discipline. The interpretable gate features $z(A)$ capture decision-relevant variation at least as well as the full raw encoding. These results support interpreting the RRM’s decompositions as disciplined, data-supported statements about procedural variation.

10 Conclusion

This paper develops a procedural approach to representing how behavior varies across a rich environment space. We introduce a *Random Rule Model* (RRM), in which predicted behavior is generated by switching among a small library of transparent, deterministic decision rules, disciplined by an activity criterion. A differentiable gating mechanism maps interpretable summary statistics into rule propensities, producing an explicitly interpretable mixture over named lines of conduct. We develop an identification theory for RRMs, showing that global identification follows from two verifiable conditions on the observed menu support - within-feature variation in decisive-side patterns and affine richness - both directly checkable on the data.

Applied to 9,831 binary lottery menus from the `choices13k` dataset, rule-gating substantially outperforms structured neural benchmarks, closing about 87% of the baseline-to-MOT (Mixture of Theories) gap while remaining highly restrictive under permutation-fit tests. The model exports well to CPC18 without re-tuning, in contrast to the most flexible benchmark, which deteriorates

sharply out of domain. Mechanism diagnostics reveal that a small subset of procedures - extreme-outcome screening, salience-based comparisons, and modal-outcome comparisons - drives most of the predictive content, with systematic reallocation along complexity and risk asymmetry. Both identification conditions are verified on the data, and a battery of robustness checks confirms that findings are not driven by the ex-ante library choice, marginal dominance relationships, or generic model flexibility.

More broadly, the RRM brings economic interpretability into high-dimensional prediction without reverting to a single valuation model. The framework may be portable beyond risky choice to settings with rich environment spaces and repeated behavior: consumer choice, dynamic decision problems, strategic settings, or social choice. Natural extensions include enlarging rule libraries, incorporating richer heterogeneity, and extending the identification conditions to richer gate parameterizations.

References

- Aguiar, V. H., Kashaev, N., and Ryan, S. P. (2023). Random utility and limited consideration. *Quantitative Economics*, 14(1):1–46.
- Arrieta, G. and Nielsen, K. (2024). Procedural Decision-Making In The Face Of Complexity. Technical report.
- Aumann, R. J. (2008). Rule-rationality versus act-rationality. Discussion Paper Series dp497, The Federmann Center for the Study of Rationality, the Hebrew University, Jerusalem.
- Aumann, R. J. (2019). A synthesis of behavioural and mainstream economics. *Nature Human Behaviour*, 3(7):666–670.
- Bell, D. E. (1985). Disappointment in decision making under uncertainty. *Operations Research*, 33(1):1–27.
- Bordalo, P., Gennaioli, N., and Shleifer, A. (2012). Salience Theory of Choice Under Risk. *The Quarterly Journal of Economics*, 127(3):1243–1285.
- Cattaneo, M. D., Ma, X., Masatlioglu, Y., and Suleymanov, E. (2020). A random attention model. *Journal of Political Economy*, 128(7):2796–2836.
- Cherepanov, V., Feddersen, T., and Sandroni, A. (2013). Rationalization. *Theoretical Economics*, 8(3):775–800.
- Enke, B. and Shubatt, C. (2023). Quantifying lottery choice complexity. Working Paper 31677, National Bureau of Economic Research.
- Erev, I., Ert, E., Plonsky, O., Cohen, D., and Cohen, O. (2017). From anomalies to forecasts: Toward a descriptive model of decisions under risk, under ambiguity, and from experience. *Psychological Review*, 124(4):369–409.
- Erev, I., Ert, E., Roth, A. E., Haruvy, E., Herzog, S. M., Hau, R., Hertwig, R., Stewart, T., West, R., and Lebiere, C. (2010). A choice prediction competition: Choices from experience and from description. *Journal of Behavioral Decision Making*, 23(1):15–47.

- Fudenberg, D., Gao, W., and Liang, A. (2026). How flexible is that functional form? quantifying the restrictiveness of theories. *The Review of Economics and Statistics*, 108(1):194–209.
- Fudenberg, D., Kleinberg, J., Liang, A., and Mullainathan, S. (2022). Measuring the completeness of economic models. *Journal of Political Economy*, 130(4):956–990.
- Fudenberg, D. and Liang, A. (2020). Machine learning for evaluating and improving theories. *ACM SIGecom Exchanges*, 18(1):4–11.
- Fudenberg, D. and Puri, I. (2022). Simplicity and probability weighting in choice under risk. *AEA Papers and Proceedings*, 112:pp. 421–425.
- Gul, F. (1991). A theory of disappointment aversion. *Econometrica*, 59(3):667–686.
- Halevy, Y. and Mayraz, G. (2024). Identifying rule-based rationality. *The Review of Economics and Statistics*, 106(5):1369–1380.
- Kahneman, D., Slovic, P., and Tversky, A. (1982). *Judgment under Uncertainty: Heuristics and Biases*. Cambridge University Press.
- Kahneman, D. and Tversky, A. (1979). Prospect theory: An analysis of decision under risk. *Econometrica*, 47(2):263–291.
- Kőszegi, B. and Rabin, M. (2006). A model of reference-dependent preferences. *Quarterly Journal of Economics*, 121(4):1133–1165.
- Kitamura, Y. and Stoye, J. (2018). Nonparametric analysis of random utility models. *Econometrica*, 86(6):1883–1909.
- Liang, A. (2025). Using machine learning to generate, clarify, and improve economic models. Papers 2508.19136, arXiv.org.
- Loomes, G. and Sugden, R. (1982). Regret theory: An alternative theory of rational choice under uncertainty. *Economic Journal*, 92(368):805–824.
- Loomes, G. and Sugden, R. (1986). Disappointment and dynamic consistency in choice under uncertainty. *Review of Economic Studies*, 53(2):271–282.
- Manzini, P. and Mariotti, M. (2007). Sequentially rationalizable choice. *American Economic Review*, 97(5):1824–1839.
- Manzini, P. and Mariotti, M. (2012). Categorize then choose: Boundedly rational choice and welfare. *Journal of the European Economic Association*, 10(5):1141–1165.
- Manzini, P. and Mariotti, M. (2014). Stochastic choice and consideration sets. *Econometrica*, 82(3):1153–1176.
- Masatlioglu, Y., Nakajima, D., and Ozbay, E. Y. (2012). Revealed attention. *American Economic Review*, 102(5):2183–2205.

- McFadden, D. and Richter, K. (1991). Stochastic rationality and revealed stochastic preference. In Chipman, J., McFadden, D., and Richter, K., editors, *Preferences, uncertainty, and rationality*, pages 161–186. Westview Press, Boulder.
- McFadden, D. L. (2006). Revealed stochastic preference: a synthesis. In Aliprantis, C. D., Matzkin, R. L., McFadden, D. L., Moore, J. C., and Yann, N. C., editors, *Rationality and Equilibrium*, Studies in Economic Theory, pages 1–20. Springer.
- Papke, L. E. and Wooldridge, J. M. (1996). Econometric methods for fractional response variables with an application to 401(k) plan participation rates. *Journal of Applied Econometrics*, 11(6):619–632.
- Peterson, J. C., Bourgin, D. D., Agrawal, M., Reichman, D., and Griffiths, T. L. (2021). Using large-scale experiments and machine learning to discover theories of human decision-making. *Science*, 372(6547):1209–1214.
- Peysakhovich, A. and Naecker, J. (2017). Using methods from machine learning to evaluate behavioral models of choice under risk and ambiguity. *Journal of Economic Behavior & Organization*, 133(C):373–384.
- Plonsky, O., Erev, I., and Ert, E. (2017). Calibration data for choice prediction competition 2018 (cpc18).
- Plonsky, O., Hazan, T., and Tennenholtz, M. (2016). Psychological forest: Predicting human behavior. *SSRN Electronic Journal*.
- Prelec, D. (1998). The probability weighting function. *Econometrica*, 66(3):497–527.
- Puri, I. (2025). Simplicity and risk. *The Journal of Finance*, 80(2):1029–1080.
- Rubinstein, A. (1988). Similarity and decision-making under risk (is there a utility theory resolution to the allais paradox?). *Journal of Economic Theory*, 46(1):145–153.
- Rubinstein, A. and Salant, Y. (2006). A model of choice from lists. *Theoretical Economics*, 1(1):3–17.
- Salant, Y. and Rubinstein, A. (2008). (a, f): Choice with frames. *The Review of Economic Studies*, 75(4):1287–1296.
- Salant, Y. and Rubinstein, A. (2011). Menu dependence and revealed preference. *Quarterly Journal of Economics*, 126(3):1333–1371.
- Selten, R. (1991). Properties of a measure of predictive success. *Mathematical Social Sciences*, 21(2):153–167.
- Seror, A. (2026). Decision rules in choice under risk.
- Simon, H. A. (1955). A behavioral model of rational choice. *The Quarterly Journal of Economics*, 69(1):99–118.
- Tversky, A. and Kahneman, D. (1974). Judgment under uncertainty: Heuristics and biases. *Science*, 185(4157):1124–1131.

Tversky, A. and Kahneman, D. (1992). Advances in prospect theory: Cumulative representation of uncertainty. *Journal of Risk and Uncertainty*, 5(4):297–323.

Online Appendix

A General Procedural Mixture Framework

This section presents the Conditional Activity Random Rule Model (CA-RRM) and its identification theory in a general discrete choice environment with finitely many alternatives per menu. The binary lottery application in the main text is a special case obtained by setting $|A| = 2$ for all menus and instantiating the dominance preorder as first-order stochastic dominance.

A.1 Choice environment

Let \mathcal{M} denote a finite collection of *menus* (choice sets). Each menu $A \in \mathcal{M}$ is a finite set of alternatives with $|A| = n_A \geq 2$. For each menu A and alternative $i \in A$, let $p(i | A) \in (0, 1)$ denote the population choice probability, with $\sum_{i \in A} p(i | A) = 1$.

Assumption 1 (Interior probabilities). For every $A \in \mathcal{M}$ and $i \in A$, $p(i | A) > 0$.

This ensures that log-ratios of choice probabilities are well defined.

A.2 Procedural library and activity

Let $\mathcal{F} = \{f_1, \dots, f_F\}$ be a finite library of *deterministic decision procedures* (rules). Each rule $f \in \mathcal{F}$ is equipped with:

- (i) An *activity set* $\mathcal{A}_f \subseteq \mathcal{M}$: the menus at which rule f delivers a strict ranking of alternatives. Define the activity indicator $\mathbf{1}_f(A) := \mathbf{1}\{A \in \mathcal{A}_f\}$.
- (ii) A *recommendation mapping* $r_f : \mathcal{A}_f \rightarrow \bigcup_{A \in \mathcal{M}} A$ such that $r_f(A) \in A$ for each $A \in \mathcal{A}_f$: the unique alternative that rule f recommends at menu A when active.

Activity is determined by an exogenous criterion (e.g., stochastic dominance of perceived lotteries in risky choice, present-value dominance in intertemporal choice, or welfare dominance in allocation problems). The key discipline is that a rule contributes to predicted choice probabilities *only* at menus where it is active.

For each menu A and alternative $i \in A$, define the *recommending set*

$$\mathcal{I}_i(A) := \{f \in \mathcal{F} : \mathbf{1}_f(A) = 1, r_f(A) = i\}, \tag{A.1}$$

the set of active rules that recommend alternative i at menu A . The set of all active rules at A is $\mathcal{F}_A := \bigcup_{i \in A} \mathcal{I}_i(A)$.

A.3 The CA-RRM

A *Conditional Activity Random Rule Model* assigns to each menu A a probability distribution $\{q_f(A)\}_{f \in \mathcal{F}} \in \Delta^{F-1}$ over rules. Define the conditional-on-activity weight of rule f :

$$\tilde{q}_f(A) := \frac{q_f(A) \mathbf{1}_f(A)}{\sum_{g \in \mathcal{F}} q_g(A) \mathbf{1}_g(A)}, \quad (\text{A.2})$$

whenever $\mathcal{F}_A \neq \emptyset$. The CA-RRM choice probability is

$$P(i | A; q) = \sum_{f \in \mathcal{I}_i(A)} \tilde{q}_f(A) = \frac{\sum_{f \in \mathcal{I}_i(A)} q_f(A)}{\sum_{g \in \mathcal{F}_A} q_g(A)}. \quad (\text{A.3})$$

Equation (A.3) expresses predicted choice as a mixture over deterministic rule recommendations, conditional on activity.

A.4 Softmax gating parameterization

The CA-RRM becomes a parametric model when $q(A)$ is generated by a differentiable gate. Let $\psi(A) \in \mathbb{R}^d$ be an observable feature vector for menu A . The *softmax gate* sets

$$q_f(A; \theta) := \frac{\exp(u_f(A; \theta))}{\sum_{g \in \mathcal{F}} \exp(u_g(A; \theta))}, \quad (\text{A.4})$$

where $u_f(A; \theta) := \alpha_f + \beta_f^\top \psi(A)$ is an affine score, and $\theta := \{(\alpha_f, \beta_f)\}_{f \in \mathcal{F}}$ collects all gate parameters.

Substituting (A.4) into (A.3) and canceling the common denominator of the softmax, the CA-RRM choice probability simplifies to

$$P(i | A; \theta) = \frac{\sum_{f \in \mathcal{I}_i(A)} \exp(u_f(A; \theta))}{\sum_{g \in \mathcal{F}_A} \exp(u_g(A; \theta))}. \quad (\text{A.5})$$

This is a *grouped softmax* over active rules, with groups defined by the alternative each rule recommends.

A.5 Normalization

The softmax is invariant to adding a common affine function to all scores: if $u_f \mapsto u_f + a + c^\top \psi$ for all f , the probabilities in (A.5) are unchanged. We therefore impose a location normalization by fixing one baseline rule $f_0 \in \mathcal{F}$ and setting

$$(\alpha_{f_0}, \beta_{f_0}) = (0, \mathbf{0}). \quad (\text{A.6})$$

Let $\vartheta \in \mathbb{R}^K$ denote the vector of free parameters, with $K = (F - 1)(1 + d)$.

A.6 Identification map and sufficient-variation condition

Multi-sided menus. Say that a menu A is *multi-sided* if at least two distinct alternatives are recommended by some active rule:

$$|\{i \in A : \mathcal{I}_i(A) \neq \emptyset\}| \geq 2.$$

Let $\mathcal{M}_{\text{ms}} \subseteq \mathcal{M}$ denote the set of multi-sided menus (the analogue of two-sided menus in the binary case). On menus that are not multi-sided, all active rules agree, so the CA-RRM prediction is 1 for the unanimously recommended alternative regardless of θ ; such menus carry no identifying information.

Log-ratio representation. For each multi-sided menu A , fix a reference alternative $i_0(A) \in A$ (any alternative with $\mathcal{I}_{i_0(A)} \neq \emptyset$). By Assumption 1 and (A.5), the log-ratios

$$\delta_i(A; \vartheta) := \log \frac{P(i | A; \vartheta)}{P(i_0(A) | A; \vartheta)} = \log \sum_{f \in \mathcal{I}_i(A)} \exp(u_f(A; \vartheta)) - \log \sum_{f \in \mathcal{I}_{i_0(A)}} \exp(u_f(A; \vartheta)) \quad (\text{A.7})$$

are well defined for each $i \in A \setminus \{i_0(A)\}$.

Identification map. Stack the log-ratios across all multi-sided menus and non-reference alternatives into a single vector:

$$H(\vartheta) := \left(\delta_i(A; \vartheta) \right)_{A \in \mathcal{M}_{\text{ms}}, i \in A \setminus \{i_0(A)\}} \in \mathbb{R}^D, \quad (\text{A.8})$$

where $D = \sum_{A \in \mathcal{M}_{\text{ms}}} (n_A - 1)$. Observing the population choice probabilities $\{p(i | A)\}$ on multi-sided menus is equivalent to observing $H(\vartheta)$, because the log-ratio transformation is a diffeomorphism from the interior of the simplex to $\mathbb{R}^{n_A - 1}$.

A.7 Global identification theorem

Decisive-side indicators and linear restriction. For each rule f and each alternative $i \in A$, define the decisive-side indicator

$$\kappa_f^i(A) := \mathbf{1}\{f \in \mathcal{I}_i(A)\},$$

where $\mathcal{I}_i(A)$ is the recommending set from (A.1). For each multi-sided menu A , fix a reference alternative $i_0(A)$ with $\mathcal{I}_{i_0}(A) \neq \emptyset$ and write the odds ratio

$$r_i(A) := \frac{P(i | A)}{P(i_0(A) | A)}, \quad i \in A \setminus \{i_0(A)\}.$$

Define the positive rule weights $\omega_f(x) := \exp(\alpha_f + \beta_f^\top x)$ for $x = \psi(A)$. From (A.5), the model-implied odds ratio satisfies

$$r_i(A) = \frac{\sum_{f \in \mathcal{I}_i(A)} \omega_f(x)}{\sum_{f \in \mathcal{I}_{i_0}(A)} \omega_f(x)}.$$

Cross-multiplying and collecting terms yields, for each non-reference alternative $i \in A \setminus \{i_0(A)\}$,

$$\sum_{f \in \mathcal{F}} \left(\kappa_f^i(A) - r_i(A) \kappa_f^{i_0(A)}(A) \right) \omega_f(x) = 0, \quad (\text{A.9})$$

i.e. $h_i(A)^\top \omega(x) = 0$ where $h_{i,f}(A) := \kappa_f^i(A) - r_i(A) \kappa_f^{i_0(A)}(A)$.

Theorem 2 (Global identification of the general CA-RRM). *Consider the CA-RRM with affine indices $u_f(A) = \alpha_f + \beta_f^\top \psi(A)$, $f \in \mathcal{F}$. Assume $P(i | A) \in (0, 1)$ for all $i \in A$ and all menus in the support (Assumption 1), and impose the normalization (A.6). Let $d = \dim(\psi)$. Suppose there exist $(d + 1)$ feature values $x^{(0)}, \dots, x^{(d)}$ such that:*

(G1) **Within-feature variation in decisive-side patterns:** *For each $k \in \{0, \dots, d\}$, stack the row vectors $h_i(A)^\top$ across all multi-sided menus A with $\psi(A) = x^{(k)}$ and all non-reference alternatives $i \in A \setminus \{i_0(A)\}$ into a matrix*

$$H^{(k)} := \begin{pmatrix} h_{i_1}(A_1)^\top \\ \vdots \\ h_{i_M}(A_M)^\top \end{pmatrix}.$$

Then $\text{rank}(H^{(k)}) = |\mathcal{F}| - 1$.

(G2) **Affine richness of feature values:** *The $(d + 1) \times (d + 1)$ matrix $X := \begin{pmatrix} 1 & (x^{(0)})^\top \\ \vdots & \vdots \\ 1 & (x^{(d)})^\top \end{pmatrix}$ has full rank.*

Then the full parameter vector $\{(\alpha_f, \beta_f)\}_{f \in \mathcal{F}}$ is globally identified from the population objects $\{P(i | A), \kappa^i(A), \psi(A)\}$, up to the normalization.

Proof. The proof parallels that of Theorem 1 in the main text, extended to the multinomial setting.

Step 1 (from choice probabilities to linear equations). Fix a multi-sided menu A and write $x = \psi(A)$. From (A.5), the choice probability ratio for any non-reference alternative i is

$$r_i(A) = \frac{P(i | A)}{P(i_0(A) | A)} = \frac{\sum_f \kappa_f^i(A) \omega_f(x)}{\sum_f \kappa_f^{i_0(A)}(A) \omega_f(x)}.$$

Cross-multiplying yields the linear restriction (A.9): $h_i(A)^\top \omega(x) = 0$, where the coefficients $h_{i,f}(A) = \kappa_f^i(A) - r_i(A) \kappa_f^{i_0(A)}(A)$ are determined by the decisive-side indicators and the observed odds ratio.

Step 2 (identifying $\omega(x)$ at a fixed feature value up to scale). Fix $k \in \{0, \dots, d\}$. All menus A with $\psi(A) = x^{(k)}$ share the same unknown weight vector $\omega(x^{(k)})$, while the decisive-side indicators may vary across menus even at the same feature value. Stacking all rows $h_i(A)^\top$ from these menus into $H^{(k)}$ gives $H^{(k)}\omega(x^{(k)}) = 0$. By (G1), $\text{rank}(H^{(k)}) = |\mathcal{F}| - 1$, so the nullspace is one-dimensional. Since all entries of $\omega(x^{(k)})$ are positive, the weight vector is identified up to a positive scalar.

Step 3 (pinning down scale using the normalization). Under (A.6), $\omega_{f_0}(x) = \exp(0 + \mathbf{0}^\top x) = 1$ for all x . Imposing $\omega_{f_0}(x^{(k)}) = 1$ uniquely pins the scalar, so $\omega(x^{(k)})$ is uniquely identified for each k .

Step 4 (recovering (α_f, β_f) from identified weights). Fix any rule f . From $\log \omega_f(x^{(k)}) = \alpha_f + \beta_f^\top x^{(k)}$ for $k = 0, \dots, d$, we obtain the linear system $(\log \omega_f(x^{(0)}), \dots, \log \omega_f(x^{(d)}))^\top = X(\alpha_f, \beta_f^\top)^\top$. By (G2), X is invertible, so (α_f, β_f) is uniquely determined. Since f was arbitrary, global identification holds. \square

Remark 1. The binary application in the main text (Theorem 1) is the special case with $|A| = 2$, where each menu produces a single row $h(A)^\top$ and the odds ratio reduces to $p(A)/(1 - p(A))$.

A.8 Local identification theorem

Remark 2. Theorem 2 above establishes global identification under conditions (G1)–(G2), which require that multiple menus share the same feature value. The following local result provides an alternative characterization based on the Jacobian of the identification map. It is particularly relevant when the gate operates on a high-dimensional feature map (such as the raw menu encoding $\psi(A) \in \mathbb{R}^{4M}$) for which the replication condition in (G1) may not hold. See Appendix O for further discussion.

Theorem 3 (Local identification of the general CA-RRM). *Impose the normalization (A.6) and let $\vartheta^* \in \mathbb{R}^K$ be any parameter vector. Define the Jacobian*

$$J(\vartheta^*) := \left. \frac{\partial H(\vartheta)}{\partial \vartheta^\top} \right|_{\vartheta = \vartheta^*} \in \mathbb{R}^{D \times K}.$$

(a) If $J(\vartheta^*)$ has full column rank K , then ϑ^* is locally identified from $\{p(i | A)\}_{A \in \mathcal{M}_{\text{ms}}}$: there exists a neighborhood $U \ni \vartheta^*$ such that $H(\vartheta) = H(\vartheta^*)$ and $\vartheta \in U$ imply $\vartheta = \vartheta^*$.

(b) If $\text{rank}(J(\vartheta^*)) = r < K$, then the null space $\mathcal{N}(J(\vartheta^*))$ has dimension $K - r$, and H is locally constant to first order along these $K - r$ linearly independent directions. If, additionally, the rank of $J(\vartheta)$ equals r on a neighborhood of ϑ^* , then by the constant-rank theorem the level set $\{\vartheta : H(\vartheta) = H(\vartheta^*)\}$ is locally a smooth embedded submanifold of dimension $K - r$ with tangent space $\mathcal{N}(J(\vartheta^*))$.

Proof. Each score $u_f(A; \vartheta)$ is affine in ϑ , and the log-sum-exp function is C^∞ on \mathbb{R}^n for any $n \geq 1$. Therefore $\delta_i(A; \vartheta)$ in (A.7), being a difference of two log-sum-exp functions composed with affine maps, is C^∞ in ϑ . The identification map H is thus a C^∞ map from \mathbb{R}^K to \mathbb{R}^D .

For part (a): if $J(\vartheta^*)$ has rank K , then by the inverse function theorem (applied to any K -dimensional subvector of H whose sub-Jacobian has rank K), H is locally injective at ϑ^* . Hence $H(\vartheta) = H(\vartheta^*)$ implies $\vartheta = \vartheta^*$ in a neighborhood.

For part (b): the first-order statement follows directly from $\text{rank}(J(\vartheta^*)) = r$: by the rank-nullity theorem, $\mathcal{N}(J(\vartheta^*))$ has dimension $K - r$, and for any $v \in \mathcal{N}(J(\vartheta^*))$, the directional derivative $DH(\vartheta^*) \cdot v = 0$. If, additionally, $\text{rank}(J(\vartheta)) = r$ on a neighborhood of ϑ^* , the constant-rank theorem yields the stronger geometric conclusion that the level set is locally a smooth $(K - r)$ -dimensional submanifold. Without this local constancy assumption, the first-order characterization still holds but the level set may have dimension less than $K - r$. \square

A.9 Closed-form Jacobian

We derive the Jacobian entries in closed form. For each active rule $f \in \mathcal{F}_A$, define the *within-side softmax share*

$$s_f(A; \vartheta) := \frac{\exp(u_f(A; \vartheta))}{\sum_{g \in \mathcal{F}_A} \exp(u_g(A; \vartheta))}, \quad (\text{A.10})$$

and for each alternative $i \in A$, write $S_i(A; \vartheta) := \sum_{f \in \mathcal{I}_i(A)} s_f(A; \vartheta)$ for the total share allocated to alternative i . Note that $P(i | A; \vartheta) = S_i(A; \vartheta)$.

Proposition 4 (Jacobian entries). *For any multi-sided menu $A \in \mathcal{M}_{\text{ms}}$, any non-reference alternative $i \in A \setminus \{i_0(A)\}$, and any free rule $f \neq f_0$:*

$$\frac{\partial \delta_i(A)}{\partial \alpha_f} = \frac{s_f(A) \mathbf{1}\{f \in \mathcal{I}_i(A)\}}{S_i(A)} - \frac{s_f(A) \mathbf{1}\{f \in \mathcal{I}_{i_0}(A)\}}{S_{i_0}(A)}, \quad (\text{A.11})$$

$$\frac{\partial \delta_i(A)}{\partial \beta_f} = \left(\frac{s_f(A) \mathbf{1}\{f \in \mathcal{I}_i(A)\}}{S_i(A)} - \frac{s_f(A) \mathbf{1}\{f \in \mathcal{I}_{i_0}(A)\}}{S_{i_0}(A)} \right) \psi(A)^\top. \quad (\text{A.12})$$

If $f \notin \mathcal{F}_A$ (i.e., f is inactive at A), then $s_f(A) = 0$ and both derivatives vanish.

Proof. From (A.7), $\delta_i(A; \vartheta) = \log N_i(A) - \log N_{i_0}(A)$, where $N_j(A) := \sum_{g \in \mathcal{I}_j(A)} \exp(u_g(A))$. For $f \in \mathcal{I}_i(A)$:

$$\frac{\partial \log N_i(A)}{\partial \alpha_f} = \frac{\exp(u_f(A))}{N_i(A)} = \frac{s_f(A) \cdot Z(A)}{N_i(A)} = \frac{s_f(A)}{S_i(A)},$$

where $Z(A) := \sum_{g \in \mathcal{F}_A} \exp(u_g(A))$ and $S_i(A) = N_i(A)/Z(A)$. For $f \notin \mathcal{I}_i(A)$, the derivative is zero. Combining the contributions from the two log terms and noting $\partial u_f / \partial \beta_f = \psi(A)^\top$ gives (A.11)–(A.12). \square

Block structure. The Jacobian $J(\vartheta^*) \in \mathbb{R}^{D \times K}$ has $(F - 1)$ column blocks, one per free rule. Each block has $1 + d$ columns (intercept α_f plus slopes β_f). The derivative for rule f at menu A is nonzero only if f is active at A and belongs to $\mathcal{I}_i(A) \cup \mathcal{I}_{i_0}(A)$, i.e., f recommends either alternative i or the reference $i_0(A)$. Variation in which rules fall on which “side” across menus—i.e., rule switching—produces sign changes in the Jacobian entries, which tends to increase rank.

Binary environments as a special case When every menu has exactly two alternatives $A = \{L^1, L^2\}$, the log-ratio representation reduces to a single log-odds per menu:

$$\delta(A; \vartheta) = \log \frac{P(L^1 | A)}{P(L^2 | A)}.$$

Setting $i = L^1$ and $i_0 = L^2$, the recommending sets become $\mathcal{I}_{L^1}(A) = \mathcal{I}_L(A)$ and $\mathcal{I}_{L^2}(A) = \mathcal{I}_R(A)$ in the notation of the main text. The Jacobian entries (A.11)–(A.12) specialize to

$$\frac{\partial \delta(A)}{\partial \alpha_f} = \frac{s_f(A) \mathbf{1}\{f \in \mathcal{I}_L(A)\}}{S_L(A)} - \frac{s_f(A) \mathbf{1}\{f \in \mathcal{I}_R(A)\}}{S_R(A)},$$

where $S_L(A) = P(L^1 | A)$ and $S_R(A) = P(L^2 | A)$. Because $s_f(A)/S_L(A)$ is the within-left softmax share $s_{L,f}(A)$ in the main text and $s_f(A)/S_R(A)$ is $s_{R,f}(A)$, this recovers

$$\frac{\partial \delta(A)}{\partial \alpha_f} = s_{L,f}(A) - s_{R,f}(A), \quad \frac{\partial \delta(A)}{\partial \beta_f} = (s_{L,f}(A) - s_{R,f}(A)) \psi(A)^\top,$$

which recovers the Jacobian entries of the main text. The binary global identification theorem in the main text (Theorem 1) is the special case of Theorem 2 obtained by setting $|A| = 2$.

Sources of identification. The closed-form Jacobian (A.11)–(A.12) makes the identification forces transparent. Three sources of variation contribute to rank:

- (i) *Side-switching:* a rule f recommends alternative i at some menus and alternative j at others. This produces sign changes in the Jacobian column for f , preventing collinearity with columns of rules that always recommend the same side.

- (ii) *Feature variation*: richer variation in $\psi(A)$ across menus generates more linearly independent rows in the Jacobian, even holding fixed which rules recommend which alternative.
- (iii) *Compositional variation*: changes in which rules are active across menus-so that the active-rule sets \mathcal{F}_A differ-alter the softmax shares $s_f(A)$ and the grouping structure, generating additional identifying variation.

Scope of the framework. The framework applies to any environment in which (a) a finite library of deterministic procedures and (b) an exogenous activity criterion can be defined. Natural applications beyond risky choice include intertemporal choice (where rules might be “choose the option with the highest present value at discount rate ρ ” and activity is determined by present-value dominance), allocation problems (where rules might correspond to equity or efficiency criteria and activity is determined by welfare dominance), and strategic settings (where rules are response heuristics and activity reflects rationalizability or dominance-based screening).

B Proof of Theorem 1

Proof. Fix any menu A and write $x = \psi(A)$. Define the positive rule weights

$$\omega_f(x) := \exp(\alpha_f + \beta_f^\top x), \quad f \in \mathcal{F},$$

and let $\kappa_f^L(A) = \mathbf{1}\{f \in \mathcal{I}_L(A)\}$ and $\kappa_f^R(A) = \mathbf{1}\{f \in \mathcal{I}_R(A)\}$ denote whether rule f is decisive for the left or right option at A .

Step 1 (from choice probabilities to linear equations). Under the CA-RRM, the model-implied probability of choosing left at menu A is

$$p(A) = \frac{\sum_{f \in \mathcal{F}} \kappa_f^L(A) \omega_f(x)}{\sum_{f \in \mathcal{F}} \kappa_f^L(A) \omega_f(x) + \sum_{f \in \mathcal{F}} \kappa_f^R(A) \omega_f(x)}. \quad (\text{A.13})$$

Because $p(A) \in (0, 1)$, the odds ratio

$$r(A) := \frac{p(A)}{1 - p(A)} \in (0, \infty)$$

is well-defined. Using (A.13), the odds can be written as

$$r(A) = \frac{\sum_f \kappa_f^L(A) \omega_f(x)}{\sum_f \kappa_f^R(A) \omega_f(x)}.$$

Cross-multiplying yields

$$\sum_f \kappa_f^L(A) \omega_f(x) = r(A) \sum_f \kappa_f^R(A) \omega_f(x),$$

and bringing all terms to the left-hand side gives the linear restriction

$$\sum_{f \in \mathcal{F}} \left(\kappa_f^L(A) - r(A) \kappa_f^R(A) \right) \omega_f(x) = 0. \quad (\text{A.14})$$

Define the row vector $h(A) \in \mathbb{R}^{|\mathcal{F}|}$ by

$$h_f(A) := \kappa_f^L(A) - r(A) \kappa_f^R(A),$$

so (A.14) can be written compactly as

$$h(A)^\top \omega(x) = 0, \quad (\text{A.15})$$

where $\omega(x) = (\omega_f(x))_{f \in \mathcal{F}}$.

Step 2 (identifying $\omega(x)$ at a fixed feature value up to scale). Fix $k \in \{0, \dots, d\}$ and consider the menus A_{k1}, \dots, A_{kM_k} that satisfy $\psi(A_{km}) = x^{(k)}$. Crucially, the gate depends on A only through $x = \psi(A)$, so all these menus share the *same* unknown weight vector $\omega(x^{(k)})$, while the decisive-side indicators (κ^L, κ^R) (and hence $h(A)$) may vary across menus even when x is fixed. Applying (A.15) to each menu and stacking the resulting equations gives

$$\begin{pmatrix} h(A_{k1})^\top \\ \vdots \\ h(A_{kM_k})^\top \end{pmatrix} \omega(x^{(k)}) = 0, \quad \text{i.e.} \quad H^{(k)} \omega(x^{(k)}) = 0.$$

By (G1), $\text{rank}(H^{(k)}) = |\mathcal{F}| - 1$, so the nullspace of $H^{(k)}$ is one-dimensional: there exists a nonzero vector $\bar{\omega}^{(k)}$ such that every solution to $H^{(k)}\omega = 0$ is of the form $\omega = c\bar{\omega}^{(k)}$ for some scalar c . Because the model weights satisfy $\omega_f(x) > 0$, the relevant solutions have $c > 0$. Thus, the menus with $\psi(A) = x^{(k)}$ identify $\omega(x^{(k)})$ up to a positive multiplicative scale factor.

Step 3 (pinning down scale using the normalization). Under the normalization $(\alpha_{f_0}, \beta_{f_0}) = (0, 0)$ we have, for all x ,

$$\omega_{f_0}(x) = \exp(0 + 0^\top x) = 1.$$

In particular, $\omega_{f_0}(x^{(k)}) = 1$. Since every solution to $H^{(k)}\omega = 0$ equals $c\bar{\omega}^{(k)}$, imposing the single

restriction $\omega_{f_0} = 1$ pins down c uniquely:

$$1 = \omega_{f_0}(x^{(k)}) = c \bar{\omega}_{f_0}^{(k)} \quad \Rightarrow \quad c = \frac{1}{\bar{\omega}_{f_0}^{(k)}}.$$

Hence there is a unique solution to $H^{(k)}\omega = 0$ that satisfies $\omega_{f_0} = 1$, and therefore $\omega(x^{(k)})$ is uniquely identified for each k .

Step 4 (recovering (α_f, β_f) from identified weights across k). Fix any rule $f \in \mathcal{F}$. From the definition of $\omega_f(\cdot)$,

$$\log \omega_f(x^{(k)}) = \alpha_f + \beta_f^\top x^{(k)}, \quad k = 0, \dots, d.$$

Stacking these $(d + 1)$ equalities yields the linear system

$$\begin{pmatrix} \log \omega_f(x^{(0)}) \\ \vdots \\ \log \omega_f(x^{(d)}) \end{pmatrix} = \begin{pmatrix} 1 & (x^{(0)})^\top \\ \vdots & \vdots \\ 1 & (x^{(d)})^\top \end{pmatrix} \begin{pmatrix} \alpha_f \\ \beta_f \end{pmatrix} = X \begin{pmatrix} \alpha_f \\ \beta_f \end{pmatrix}.$$

Assumption (G2) states that the $(d + 1)$ feature vectors $x^{(0)}, \dots, x^{(d)}$ are *affinely independent*, equivalently that the augmented regressor matrix X has full rank; hence X is invertible. Therefore (α_f, β_f) is uniquely determined. Since f was arbitrary, this holds for all $f \in \mathcal{F}$, establishing global identification (up to the imposed normalization). \square

C Attention-Rule Removal

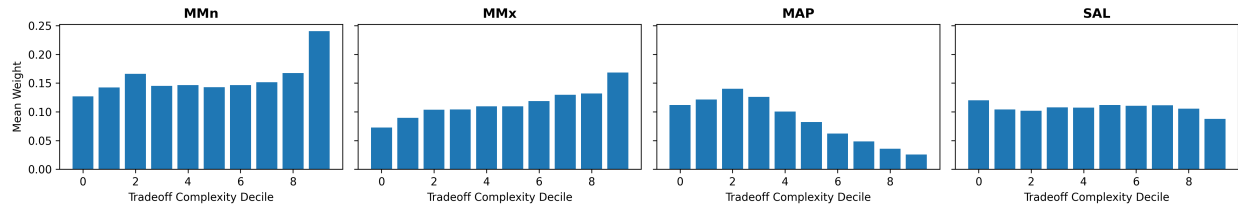
Table A.1 replicates the main cross-validation comparison (Table 1) with the rule-gating model restricted to the 10 economic rules (excluding A1/A2).

Table A.1: Robustness: predictive performance after removing attention defaults A1/A2. Rule-gating (10 rules) excludes the two attention defaults; all other models are identical to Table 1.

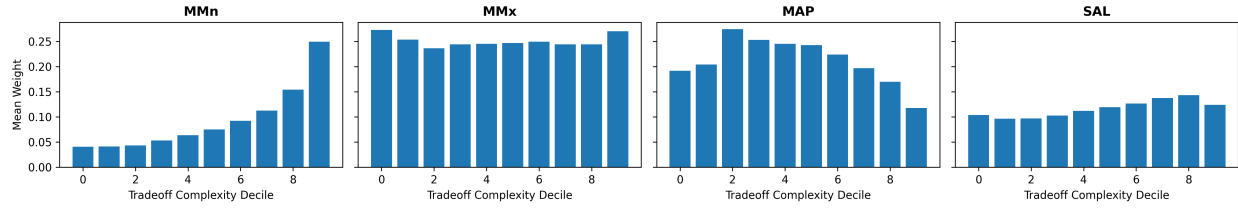
Model	Mean MSE	SD	Mean MSE _w	Best LR
MOT [†]	0.01139	0.00056	n.a.	0.001
Rule-gating	0.01282	0.00059	0.01269	0.010
Context-dependent	0.01344	0.00081	0.01330	0.010
Value-based	0.01921	0.00081	0.01904	0.010
Rule-gating (Spec A)	0.02014	0.00092	0.01999	0.010
Neural PT	0.02064	0.00085	0.02050	0.010
Neural CPT	0.02145	0.00093	0.02134	0.010
Neural EU	0.02215	0.00085	0.02205	0.010

Note: [†]MOT learning rate is selected by test MSE following the published protocol of Peterson et al. (2021). Rule-gating (Spec A) excludes A1/A2. The full 12-rule specification (Rule-gating) is reproduced from Table 1 for comparison.

Figures A.1 and A.2 replicate the complexity and risk mechanism plots (Figures 6 and 7) for MMN, MMX, MAP, SAL under the 10-rule specification (no A1/A2), compared with the full 12-rule library. The qualitative patterns persist: MMX rises with tradeoff complexity while MAP declines, and along risk asymmetry, extreme-outcome comparisons decrease while MAP increases. The removal of the attention rules reallocates their former responsibility mass to the structured rules, but the relative ordering and directional movements of the non-attention rules remain intact. This confirms that the interpretability claims from the mechanism analysis concern genuine behavioral regularities in the structured rules, not patterns induced by the presence of the attention channel.

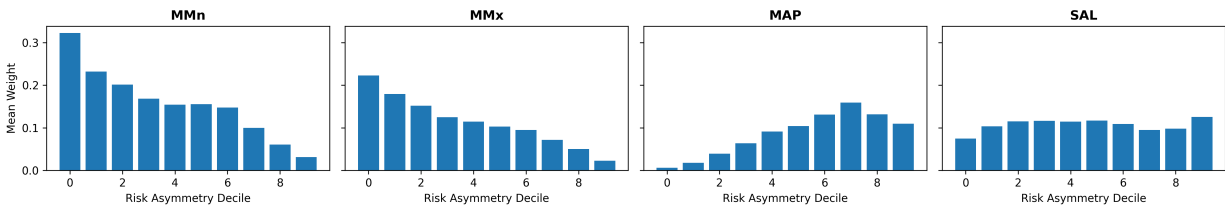


(a) Full library (12 rules).

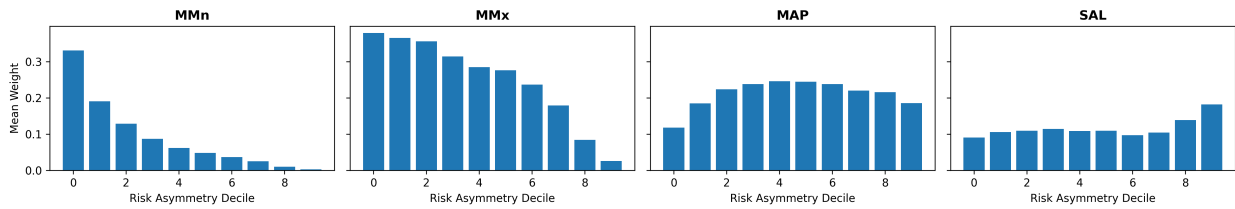


(b) 10 rules (no A1/A2).

Figure A.1: Mean effective responsibility weights across deciles of tradeoff complexity for MMn, MMx, MAP, SAL: full library vs. 10-rule specification.



(a) Full library (12 rules).



(b) 10 rules (no A1/A2).

Figure A.2: Mean effective responsibility weights across deciles of risk asymmetry for MMn, MMx, MAP, SAL: full library vs. 10-rule specification.

D Additional Figures

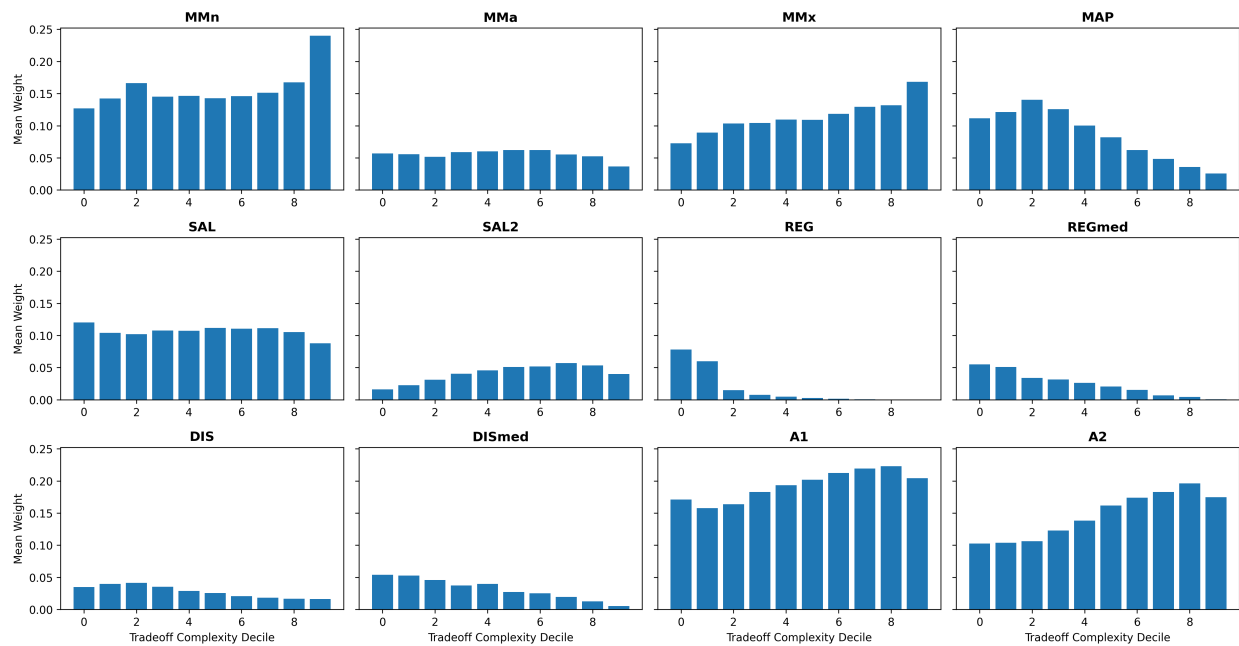


Figure A.3: Mean effective usage weights across deciles of tradeoff complexity $\text{Comp}(A)$ for all rules.

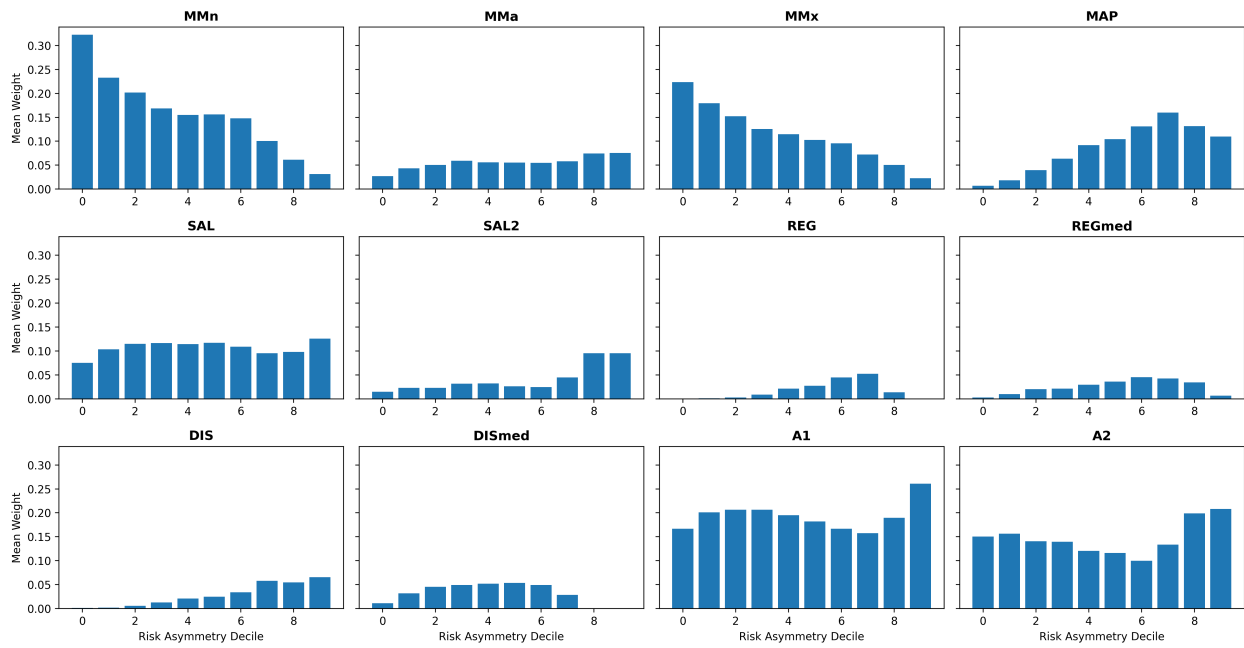


Figure A.4: Mean effective usage weights across deciles of risk asymmetry $\text{RiskAsym}(A)$ for all rules.

Table A.2: Paired comparisons of models against the rule-gating model (fold-level deltas). Positive delta means the comparison model performs worse. SE is split-to-split standard error.

Model A	vs.	Metric	Mean delta	SE	N folds
Context-dependent	Rule-gating	test_mse	-0.00120	0.00011	50
Neural CPT	Rule-gating	test_mse	0.00681	0.00013	50
Neural EU	Rule-gating	test_mse	0.00751	0.00012	50
Neural PT	Rule-gating	test_mse	0.00599	0.00013	50
Rule-gating	Rule-gating	test_mse	-0.00183	0.00006	50
Value-based	Rule-gating	test_mse	0.00457	0.00012	50
MOT	Rule-gating	test_mse	-0.00325	0.00011	50

E Paired Comparisons

Table A.2 reports split-level comparisons for out-of-sample performance. For each pair of models, we compute the per-split difference in test MSE and report the mean and standard error across the 50 random splits. Because the train/test splits overlap across repetitions, these standard errors should be interpreted as descriptive measures of split-to-split variability rather than formal sampling-based inference.

F Model-Level Uncertainty Intervals

Table A.3 reports split-variability intervals ($\text{mean} \pm 1.96 \times \text{SE}$) for each model’s out-of-sample metrics, constructed from fold-to-fold variability across the 50 CV splits. These intervals are descriptive summaries of how performance varies across train/test partitions, not formal confidence intervals.

Table A.3: Model-level split-variability intervals from fold-to-fold variability (50 splits).

Model	Mean MSE	SE	CI low	CI high
MOT	0.01139	0.00008	0.01124	0.01155
Rule-gating	0.01282	0.00008	0.01266	0.01298
Context-dependent	0.01344	0.00012	0.01322	0.01367
Value-based	0.01921	0.00011	0.01898	0.01943
Neural PT	0.02064	0.00012	0.02040	0.02087
Neural CPT	0.02145	0.00013	0.02119	0.02171
Neural EU	0.02215	0.00012	0.02192	0.02239

Note: Intervals computed as $\text{mean} \pm 1.96 \times \text{SE}$, where $\text{SE} = \text{SD} / \sqrt{n_{\text{folds}}}$. These are descriptive split-variability intervals, not formal confidence intervals.

G Ablation Effect Split-Variability Intervals

Table A.4 reports split-variability intervals for the absolute ablation effect $\Delta\text{MSE} = \text{MSE}^{-f} - \text{MSE}^{\text{full}}$, constructed from fold-to-fold variability. For each rule f , we compute the per-fold MSE increase from dropping rule f from the full 12-rule library, then report the mean, standard error, and interval bounds. (The relative index $\phi(f) = \Delta\text{MSE}/\text{MSE}^{\text{full}}$, as defined in Equation (16), is reported in Table A.5.)

The near-identical ablation effects for MMA, REG, and REGMED are not a computational artifact: these three rules have very small and noisy effects because they are largely substitutable with the other rules in the library. Their ablation impacts are indistinguishable at the reported precision.

Table A.4: Ablation effect (absolute MSE change) with split-variability intervals from fold-to-fold variability. Each rule is ablated from the full 12-rule library.

Rule	Mean ΔMSE	SE	CI low	CI high
SAL2	0.00095	0.00006	0.00083	0.00108
SAL	0.00075	0.00005	0.00065	0.00085
MMX	0.00067	0.00005	0.00057	0.00077
MMN	0.00032	0.00004	0.00024	0.00040
REGMED	0.00031	0.00004	0.00023	0.00039
REG	0.00025	0.00004	0.00016	0.00034
DIS	0.00017	0.00003	0.00011	0.00024
DISMED	0.00015	0.00003	0.00008	0.00022
MAP	0.00013	0.00003	0.00007	0.00020
MMA	0.00003	0.00003	-0.00002	0.00009

Note: $\Delta\text{MSE} = \text{MSE}^{-f} - \text{MSE}^{\text{full}}$: absolute MSE increase when rule f is dropped (fold-level paired differences). The relative index $\phi(f) = \Delta\text{MSE}/\text{MSE}^{\text{full}}$ is reported in Table A.5.

H Decomposition Stability

Table A.5 reports the stability of the responsibility weights w_f and ablation index $\phi(f)$ across the 50 CV folds. For each rule, we report the mean, standard deviation, and coefficient of variation ($\text{CV} = \text{SD}/\text{mean}$) across folds. The Spearman rank correlations reported in the table note summarize the stability of the *orderings*: for all $\binom{50}{2}$ fold pairs, we compute the Spearman correlation between the fold-level w_f (or $\phi(f)$) vectors, and report the mean, minimum, and maximum.

Table A.5: Decomposition stability across 50 CV folds. For each rule f : mean, standard deviation, and coefficient of variation (CV) of the responsibility weight w_f and ablation index $\phi(f)$ across folds.

Rule	Mean w_f	SD w_f	CV w_f	Mean $\phi(f)$	SD $\phi(f)$	CV $\phi(f)$
A2	0.2333	0.0118	0.05	—	—	—
A1	0.2057	0.0121	0.06	—	—	—
MMX	0.1214	0.0067	0.06	0.0557	0.0278	0.50
SAL	0.1059	0.0045	0.04	0.0626	0.0305	0.49
REG	0.0628	0.0049	0.08	0.0207	0.0262	1.26
MAP	0.0590	0.0068	0.11	0.0112	0.0195	1.74
MMN	0.0574	0.0225	0.39	0.0266	0.0220	0.83
REGMED	0.0508	0.0110	0.22	0.0255	0.0241	0.95
SAL2	0.0416	0.0023	0.05	0.0794	0.0372	0.47
DISMED	0.0296	0.0070	0.24	0.0125	0.0192	1.54
DIS	0.0237	0.0100	0.42	0.0144	0.0194	1.35
MMA	0.0088	0.0039	0.45	0.0029	0.0158	5.47

Note: Spearman rank correlation of w_f orderings across all fold pairs: mean $\rho = 0.935$, range [0.776, 1.000].
Spearman rank correlation of $\phi(f)$ orderings: mean $\rho = 0.564$, range [-0.794, 0.976].

I Selection Stability

Table A.6 reports the frequency with which each behavioral rule is selected in the top- k set across the 50 cross-fitted CV folds. Higher frequency indicates more stable selection.

Table A.6: Cross-fitted selection stability: frequency of each behavioral rule appearing in top- k across 50 folds.

Rule	Freq. top-3	Freq. top-5	Freq. top-7	Freq. top-12
A1	1.00	1.00	1.00	1.00
A2	1.00	1.00	1.00	1.00
DIS	0.00	0.00	0.00	1.00
DISMED	0.00	0.00	0.00	1.00
MAP	0.00	0.64	1.00	1.00
MMA	0.00	0.00	0.00	1.00
MMN	0.00	0.00	0.00	1.00
MMX	0.54	1.00	1.00	1.00
REG	0.00	0.36	1.00	1.00
REGMED	0.00	0.00	0.86	1.00
SAL	0.46	1.00	1.00	1.00
SAL2	0.00	0.00	0.14	1.00

Note: Frequency 1.00 means the rule is selected in every fold.

Table A.7: Portability to CPC18: out-of-domain MSE when models are trained on `choices13k` and evaluated on CPC18 without re-tuning. Lower is better.

Model	MSE _{CPC}	MSE _{CPC} (trial-wtd)	# menus	# trials
Rule-gating	0.0170	0.0172	180	354,400
Context-dependent	0.0172	0.0178	180	354,400
Neural CPT	0.0320	0.0313	180	354,400
Neural EU	0.0320	0.0316	180	354,400
Value-based	0.0321	0.0321	180	354,400
Neural PT	0.0326	0.0322	180	354,400
MOT	0.0926	0.0892	180	354,400

J Menu-Level Portability (Legacy)

Table A.7 reports the legacy menu-level portability metrics for comparability with the prior version.

K Feature-Based Baselines: Details

We include six feature-based baselines as additional benchmarks. Each uses the same 50-fold CV protocol and evaluation metrics as the main models.

Feature sets. Three feature sets are used:

- **F1: Summary statistics** (≈ 18 dimensions): expected value, variance, standard deviation, min, max, range, and number of support points for each lottery, plus pairwise gaps (EV gap, variance gap, min gap, max gap).
- **F2: Rule features** (24 dimensions): for each menu A and each rule $f \in \mathcal{F}$, we concatenate the left-recommendation indicator $L_f(A)$ and the activity indicator $A_f(A)$.
- **F3: Combined** (≈ 42 dimensions): concatenation of F1 and F2.

Models and tuning.

- **Fractional logit:** we fit a binomial GLM with logit link (`statsmodels.GLM, family=Binomial()`) directly on the continuous choice frequency $\hat{p}(A) \in [0, 1]$, following Papke and Wooldridge (1996). The L_2 regularization parameter α is selected from $\{0, 0.01, 0.1, 1\}$ by inner-fold validation (80/20 split within training).
- **Gradient-boosted trees (GBT):** we fit `GradientBoostingRegressor` (scikit-learn) with `max_depth=4`. The number of estimators is selected from $\{100, 200, 500\}$ by inner-fold validation. The target is the continuous choice frequency $\hat{p}(A)$.

All hyperparameter selection is restricted to training folds; no CPC18 or test-set information is used.

L Placebo Rule Library

A distinct concern from library selection is whether the rule indicators themselves carry genuine predictive content, or whether the gate could achieve similar performance with *any* set of binary indicators that have the same marginal statistics. To address this, we construct a placebo test in which the rule indicators are scrambled while preserving their marginal properties.

Stratified permutation design. A naïve permutation of rule indicators across all menus would change the marginal activity and recommendation rates in ways that could trivially degrade performance. To avoid this confound, we stratify menus by a simple measure of menu complexity—the total number of support points across the two lotteries, $|\text{Supp}(L^1)| + |\text{Supp}(L^2)|$ —and permute *within* quantile bins of this variable.¹¹ Concretely, for each rule f independently and within each of 10 quantile bins, we randomly reassign the $(L_f(A), A_f(A))$ pairs across menus within that bin. This preserves, for each rule and each complexity stratum, the marginal activity rate and recommendation rate, but destroys the mapping from a specific menu to its rule indicators.

The gate architecture, training protocol (50 folds, two-pass LR selection, same number of gradient steps and batch size as the main rule-gating model), and all other inputs—including the gate features $z(A)$ —are identical. We repeat the permutation 50 times and report the average test MSE across permutations.

Results. Table A.8 reports the comparison. The placebo library produces substantially higher MSE than the real library, confirming that the rule indicators carry genuine, menu-specific predictive content that cannot be replicated by indicators with matching marginal statistics. The gate’s predictive advantage is therefore attributable to the *structured correspondence* between menu features and rule recommendations, not merely to the availability of additional binary regressors.

M Feature-Based Baselines: Results

A natural question is whether competitive performance could be achieved by a standard off-the-shelf method applied to the same features, without the gate architecture or the behavioral structure of the RRM. To address this, we train two classical machine-learning models on the same data and evaluate them under the same 50-fold CV protocol as the main models.

¹¹This support-count measure captures a basic structural feature of the menu (how many distinct outcomes appear). It differs from the tradeoff complexity $\text{TC}(A)$ used in Section 8, which isolates how much the two CDFs cross. We stratify on support count because it is the most direct determinant of rule activity patterns: rules that involve pairwise outcome comparisons (e.g., SAL, REG) mechanically depend on the number of support points.

Table A.8: Placebo rule library test. The “Real” row reports the rule-gating model with the actual rule indicators; the “Placebo” row uses stratified-permuted indicators that preserve marginal activity rates per rule per complexity bin but destroy the menu-to-indicator mapping.

Library	Mean MSE	SD	n
Real (rule-gating)	0.01282	0.00059	50
Placebo (permuted)	0.02403	0.00032	50

Note: Placebo indicators are constructed by independently permuting each rule’s (L_f, A_f) pairs across menus within quantile bins of menu complexity (number of nonzero outcomes). The gate architecture, training protocol, and all other inputs are identical to the main rule-gating model. SD for the real model is across 50 CV folds; SD for the placebo is across permutations.

Models. The first is a *fractional logit*: a binomial generalized linear model (GLM) with a logit link, where the dependent variable is the continuous menu-level choice frequency $\hat{p}(A) \in [0, 1]$ (following Papke and Wooldridge 1996). The L_2 regularization parameter adds a penalty proportional to $\lambda \|\beta\|_2^2$; λ is selected by inner-fold validation from $\{0, 0.01, 0.1, 1\}$. The second is a *gradient-boosted tree ensemble* (GBT, scikit-learn), a flexible nonparametric learner; the number of boosting rounds is selected from $\{100, 200, 500\}$ by inner-fold validation.

Feature sets. Each model is trained on three alternative feature sets: (F1) *summary statistics* (≈ 18 dimensions); (F2) *rule indicators* (24 dimensions); and (F3) the *concatenation* of F1 and F2 (≈ 42 dimensions). Full details are in Appendix K.

Results. Table A.9 reports results. On rule features alone (F2), rule-gating (MSE 0.01282) substantially outperforms both the fractional logit (0.02346) and GBT (0.02039). The comparison does not isolate architecture from features (rule-gating also conditions on $z(A)$), but it shows that the activity-conditioned softmax gate extracts substantially more predictive content from the rule library than standard off-the-shelf methods.

GBT on summary statistics (F1, MSE 0.00997) and on combined features (F3, MSE 0.00957) outperform all structured models by an important margin. This shows that rich predictive information exists in the raw lottery features, and that a sufficiently flexible learner can exploit it. However, GBT produces an opaque mapping with no behavioral decomposition. Rule-gating therefore occupies a distinct niche: among all models that produce a transparent behavioral decomposition, it delivers the strongest prediction.

N Raw-Encoding Gate Benchmark

As a robustness check, we estimate a variant in which the softmax gate operates on the raw menu encoding $\psi(A) \in \mathbb{R}^{4M}$ (Equation (21)) instead of the interpretable features $z(A)$. With $M = 10$,

Table A.9: Feature-based baselines: out-of-sample MSE (50 splits). Rules = binary rule indicators; Stats = lottery summary statistics; Combined = concatenation.

Model	Mean MSE	SD	Mean MSE _w	Features
GBT (combined)	0.00957	0.00041	0.00947	F3
GBT (stats)	0.00997	0.00041	0.00986	F1
Fractional logit (combined)	0.01579	0.00073	0.01565	F3
GBT (rules)	0.02039	0.00079	0.02013	F2
Fractional logit (rules)	0.02346	0.00103	0.02324	F2
Fractional logit (stats)	0.02362	0.00099	0.02338	F1

Note: F1 = summary statistics (≈ 18 dim); F2 = rule indicators (24 dim); F3 = combined (≈ 42 dim). All models use the same 50-fold CV protocol as Table 1.

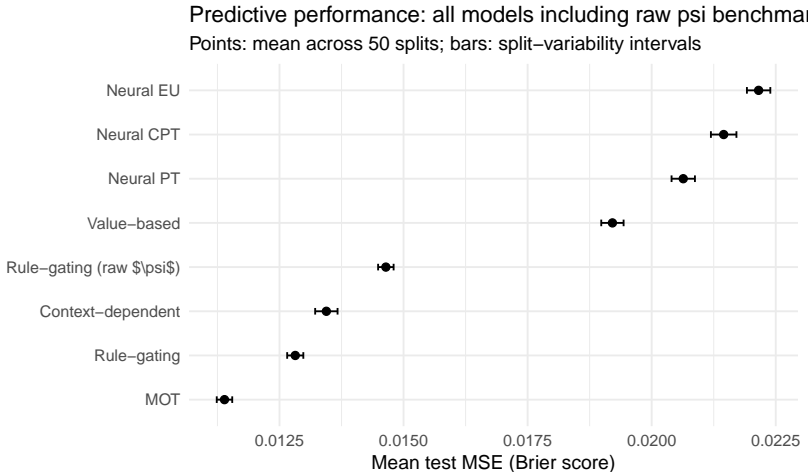


Figure A.5: Predictive performance of all models including the raw-encoding gate variant: mean test MSE across 50 random splits with split-variability intervals.

this is a 40-dimensional input, yielding $40 \times |\mathcal{F}|$ gate parameters (plus biases) instead of $12 \times |\mathcal{F}|$. Because the raw encoding is essentially injective on the menu support, the global identification conditions (G1)-(G2) of Theorem 1 are not applicable to this parameterization (see Section 6.6).

The raw-encoding gate achieves mean test MSE 0.01464, compared to 0.01282 for the baseline specification using $z(A)$ - an approximately 14% increase (Figure A.5). The 12 interpretable summary statistics therefore capture the decision-relevant variation at least as well as the raw encoding, while the additional dimensions of $\psi(A)$ appear to introduce noise. With more parameters to estimate, the raw-encoding gate is also more prone to overfitting.

O Local Identification for High-Dimensional Gate Features

The global identification conditions (G1)–(G2) of Theorems 1 and 2 require that multiple menus map to the same feature value, so that within-feature variation in decisive-side patterns can identify the rule weights. When the gate operates on the raw menu encoding $\psi(A) \in \mathbb{R}^{4M}$, which is essentially injective on the menu support, this replication condition cannot hold: each menu maps to a distinct feature value, leaving (G1) vacuous.

For such high-dimensional encodings, identification can still be assessed through the local approach of Theorem 3. At a given parameter value ϑ^* , one computes the Jacobian $J(\vartheta^*)$ of the identification map in closed form (Section A.9) and checks whether it achieves full column rank. If so, part (a) of Theorem 3 guarantees that ϑ^* is locally identified. The effective dimension of the identified parameter space can be read off from the rank: if $\text{rank}(J) = r$, then r independent parameter combinations are pinned down by the data, while the remaining $K - r$ directions lie in the tangent null space.

This local approach complements the global conditions in the following sense. The coarsened features $z(A)$ used in the baseline specification are designed to satisfy (G1)–(G2), providing global identification guarantees that do not depend on a particular parameter value. When a researcher instead uses a richer feature map for which (G1) is not applicable, the Jacobian rank diagnostic provides a parameter-value-specific check that can be evaluated at the fitted parameters. In our empirical analysis (Section 9.1), both diagnostics support identification: the global conditions (G1)–(G2) hold for the $z(A)$ specification, and the Jacobian achieves full column rank at the fitted parameters for both the $z(A)$ and raw- ψ specifications.